

Symmetry-based requirement for the measurement of electrical and thermal Hall conductivity under an in-plane magnetic field

Takashi Kurumaji¹

¹*Department of Advanced Materials Science, University of Tokyo, Kashiwa 277-8561, Japan**
(Dated: April 4, 2023)

The in-plane (thermal) Hall effect is an unconventional transverse response when the applied magnetic field is in the (heat) current plane. In contrast to the normal Hall effect, the in-plane Hall effect requires the absence of certain crystal symmetries, and possibly manifests a non-trivial topology of quantum materials. An accurate estimation of the intrinsic in-plane (thermal) Hall conductivity is crucial to identify the underlying mechanisms as in the case of the Kitaev spin-liquid candidate α -RuCl₃. Here, we give the symmetry conditions for the in-plane Hall effect and discuss the implications that may impede the experimental evaluation of the in-plane (thermal) Hall conductivity within the single-device measurement. First, the lack of symmetry in crystals can create merohedral twin domains that cancel the total Hall signal. Second, even in a twin-free crystal, the intrinsic response is potentially contaminated by the out-of-plane conduction in three-dimensional systems, which is systematically unavoidable in the in-plane Hall systems. Third, even in a quasi-two-dimensional system, the conversion of (thermal) resistivity, $\hat{\rho}$ ($\hat{\lambda}$), to (thermal) conductivity, $\hat{\sigma}$ ($\hat{\kappa}$) requires protocols beyond the widely-used simplified formula $\sigma_{xy} = \rho_{yx}/(\rho_{xx}^2 + \rho_{yy}^2)$ ($\kappa_{xy} = \lambda_{yx}/(\lambda_{xx}^2 + \lambda_{yy}^2)$) due to the lack of in-plane-rotational symmetry. In principle, two independent sample devices are necessary to accurately estimate the σ_{xy} (κ_{xy}). As a case study, we discuss the half-integer quantization of the in-plane thermal Hall effect in the spin-disordered state of α -RuCl₃. For an accurate measurement of the thermal Hall effect, it is necessary to avoid crystals with the merohedral twins contributing oppositely to κ_{xy} , while the out-of-plane transport may have a negligible effect. To deal with the field-induced rotational-symmetry breaking, we propose two symmetry-based protocols, improved single-device and two-device methods. The considerations in the manuscript are generally applicable to a broad class of materials and provide a useful starting point for understanding the unconventional aspects of the in-plane Hall effect.

INTRODUCTION.

The conventional Hall effect occurs in metals and semiconductors as a transverse electric field (E_y) in an electric current along the x axis (J_x) when the magnetic field (B) is applied along the z direction (Fig. 1(a)) [1]. This is due to the Lorentz force on the conduction electrons and the E_y changes its sign when the B_z is reversed ($E_y(-B_z) = -E_y(B_z)$). Two other types of transverse responses are known, which are induced when the magnetic field is applied in the xy plane. One of them is the planar Hall effect, which occurs when B is rotated by an angle θ from the x axis to the y axis (Fig. 1(b)) [2–4]. This is actually not a true field-odd Hall effect, but rather a field-even response resulting from the anisotropy of magnetoresistance [5]. The other is the in-plane Hall effect, which is the main interest of this study. The typical configuration is shown in Fig. 1(c), where the applied B_x is parallel to J_x and the induced E_y is reversed by the inversion of B , and thus is the field-odd response [6]. This effect has been reported experimentally in cubic germanium as the B^3 -order effect [7, 8], as well as in trigonal bismuth [9, 10], and in monoclinic binary semimetals as the B -linear effect [11, 12].

The in-plane Hall effect, or sometimes referred to as the longitudinal Hall effect, was previously recognized as a consequence of the multi-band effect [8, 12–17]. Independently from these early studies, this effect has recently attracted increasing interest in the context of a topological signature of quantum materials. Theories consider the quantization of the anomalous Hall effect by in-plane magnetization on magnetic topological insulators [18–25], the effect of the spin-orbit interaction [26, 27], and the field-induced quantization in two-dimensional electron gas [27–29]. The role of the Berry curvature in the electron bands suggests an intrinsic (dissipationless) nature of the in-plane Hall effect in topologically non-trivial semimetals [27, 30–32]. Experimentally, the in-plane Hall conductivity is suggested to be a signature of unconventional topological transports as reported in the nonmagnetic semimetal ZrTe₅ [33], heterodimensional superlattice of VS₂-VS [34], and magnetic half-Heusler DyPtBi [35]. For magnetic insulators, the in-plane thermal Hall effect has been debated to be an evidence for the chiral Majorana edge mode [36] in a Kitaev spin liquid candidate α -RuCl₃ [37–40].

Importantly, the in-plane Hall effect is a consequence of the absence of certain crystal symmetries [41–43]. This is different from the situation for the normal Hall effect, which is always allowed by the time-reversal symmetry breaking under the out-of-plane field. As a result, several factors need to be carefully considered in order to

* kurumaji@edu.k.u-tokyo.ac.jp

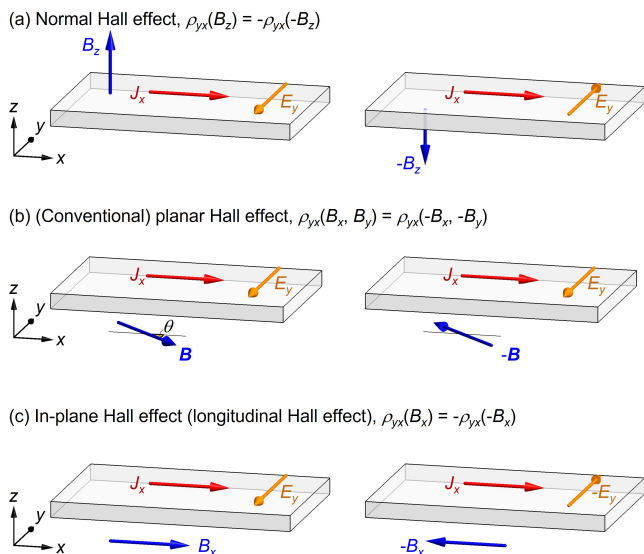


FIG. 1. Schematic configurations of (a) normal Hall effect, (b) conventional planar Hall effect, and (c) field-odd in-plane Hall effect (longitudinal Hall effect). Gray rectangle is a crystal. Blue, red, and orange arrows represent the magnetic field B , current J_x applied along the x axis, and the induced Hall electric field E_y along the y axis, respectively. xyz is the Cartesian coordinate. Left and right panels represent the E_y response to the B -field reversal.

discuss the in-plane Hall effect. In the view of the growing importance of this unconventional effect, we discuss the symmetry conditions and appropriate experimental protocols for the in-plane Hall effect, which provide a useful guide for the interpretation of the observed signal to extract the intrinsic feature of this phenomenon.

In this manuscript, we start by summarizing the symmetry requirements for the in-plane (thermal) Hall effect. We derive the absence conditions for the in-plane Hall effect by applying a pictorial approach [44], which is an extension of the previous studies to arbitrary magnetic fields in nonmagnetic and magnetic materials. It is applied to ZrTe_5 to see if the observation in Ref. [33] is allowed by symmetry.

The following three sections address the consequences of the lack of symmetries in the in-plane Hall system. First, we consider the effect of crystal twinning, which degrades the observed in-plane Hall signal. Second, we discuss the experimental protocol for estimating the in-plane Hall conductivity by the conversion between the (thermal) resistivity tensor $\hat{\rho}$ ($\hat{\lambda}$) and the conductivity tensor $\hat{\sigma}$ ($\hat{\kappa}$). We show that the in-plane Hall resistivity in a (twin-free) three-dimensional system is contaminated by the out-of-plane transport, and is not directly proportional to the intrinsic in-plane Hall conductivity. Interestingly, this effect is unavoidable due to the lack of symmetry for the in-plane Hall system. Third, we consider the quasi-two-dimensional system, where the above

effect is negligible. Even in this case, the effect of the in-plane magnetic field breaks the xy -rotational symmetry, which restricts the application of the conversion formula from $\hat{\rho}$ ($\hat{\lambda}$) to $\hat{\sigma}$ ($\hat{\kappa}$), and requires an approach beyond the conventional five-electrode method using a single device.

Finally, as a case study, we consider the thermal Hall effect in $\alpha\text{-RuCl}_3$ to see how the above factors affect the observations. We point out that the procedures used in previous work to quantify the thermal Hall conductivity potentially contain a systematic error. This is due to the breaking of the xy -rotational symmetry by the in-plane field, which has not been sufficiently verified in previous studies. We propose the improvements of the experimental protocols in order to clarify the half-integer quantization of κ_{xy} in the spin-disordered state of $\alpha\text{-RuCl}_3$.

As a note on the terminology, we emphasize that the in-plane Hall effect differs from the conventional planar Hall effect with respect to the response to the B -field reversal. In this manuscript, to follow the convention [34] and to avoid confusion, we use the term in-plane (thermal) Hall effect to refer to the field-odd response and the planar Hall effect only for the field-even response. However, a few papers use the term "planar Hall effect" [28, 30, 39, 45] to refer to the field-odd in-plane (anomalous/thermal) Hall effect. We do not follow this trend, as the term "planar Hall effect" has long been used to evoke the field-even effect, although we do not say that this wording is inappropriate [46].

THE SYMMETRY CONDITIONS OF THE IN-PLANE HALL EFFECT

Previous studies provide symmetry conditions of the in-plane Hall effect for nonmagnetic systems [42, 47, 48], for magnetic systems [43] upto the B -linear term, and for the Berry curvature terms in nonmagnetic systems [20, 32]. There is also a specific application to a honeycomb-lattice system [49]. To more intuitively capture the importance of crystal symmetry, we apply a pictorial approach [44] to obtain the necessary conditions for the in-plane Hall effect. This is useful for heuristically deriving the symmetry conditions of various phenomena such as nonreciprocal phenomena and multiferroicity [50–52] in both magnetic and nonmagnetic systems

We consider the equation, $E_y = \rho_{yx}(B_x, B_y, 0)J_x$, which relates the electric field along the y axis and the applied current along the x axis under the in-plane magnetic field $\mathbf{B} = (B_x, B_y, 0)$. We separate it into a field-even planar Hall component, $E_y^e \propto \rho_{yx}^e$ and a field-odd component, $E_y^o \propto \rho_{yx}^o$, and consider only the latter, i.e., the in-plane Hall effect. We note that the conditions for $\rho_{yx}^o = 0$ are equivalent to those for $\sigma_{xy}^o = 0$ because the form of the conductivity tensor is identical to that of the resistivity. All of these arguments hold regardless of the microscopic mechanism, and are even applicable to the

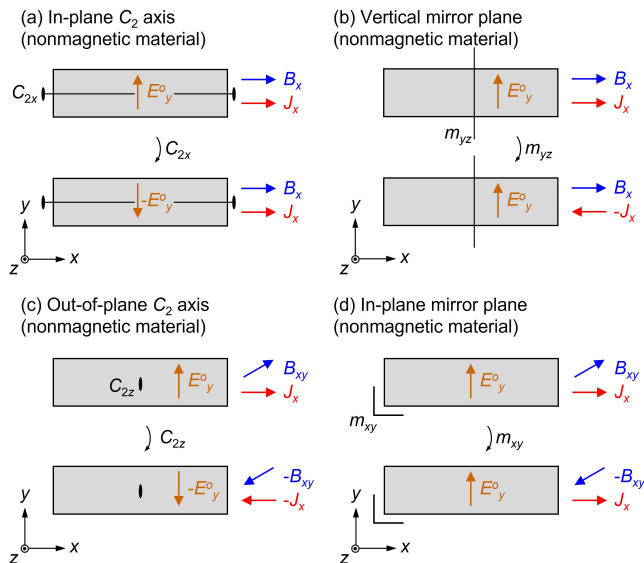


FIG. 2. Symmetry conditions for the absence of the in-plane Hall effect. Gray rectangle is a crystal. Orange arrow represents a tentative in-plane Hall electric field E_y^o proportional to $\rho_{yx}^o(B_x, B_y, 0)$, which is proved to be zero. The superscript o denotes the field-odd nature. The rotation or mirror operation for each figure transforms the top panel into the bottom panel. The symmetry operations for the zero-field state are denoted as (a) a C_2 axis along the x axis (C_{2x} , black line), (b) a vertical mirror in the yz plane (m_{yz} , black line), (c) an out-of-plane C_2 axis along the z axis (C_{2z} , black ellipse), and (d) a horizontal mirror in the xy plane (m_{xy} , black L-shape symbol).

in-plane thermal Hall effect by replacing the E_y with the temperature gradient $-\nabla_y T$, and the current J_x with the heat current.

For simplicity, we consider nonmagnetic systems in the main text, and discuss the extension to magnetic materials in SI Sec. A. We note that the in-plane Hall effect is allowed when the magnetic field is applied in an arbitrary direction with respect to the crystal axes [42], which reduces the crystal symmetry to the triclinic 1 and $\bar{1}$. We discuss rather special cases where the magnetic field is applied within a high-symmetry direction. The following four cases are the symmetry conditions for the absence of the in-plane Hall effect.

1. $\rho_{yx}^o(B_x, 0, 0)$ is zero if there is a C_2 axis along the x axis (Fig. 2(a)).
2. $\rho_{yx}^o(B_x, 0, 0)$ is zero if there is a vertical mirror symmetry m in the yz plane (Fig. 2(b)).
3. $\rho_{yx}^o(B_x, B_y, 0)$ is zero if there is a C_2 axis along the z axis (Fig. 2(c)).
4. $\rho_{yx}^o(B_x, B_y, 0)$ is zero if there is a horizontal mirror symmetry m in the xy plane (Fig. 2(d)).

Figures 2 provide how these above conditions are validated. The top panel for each figure can be converted to the bottom one through the symmetry operation, which proves that ρ_{yx}^o . We consider the condition 1 as an example. Figure 2(a) considers that the sample has the C_2 axis along the x axis and current flows along the x axis under a magnetic field parallel to x axis. We assume that the crystal has an intrinsic symmetry C_2 along the x axis in zero field, and the applied field along x does not break the symmetry (e.g., field-induced nematic/CDW/SDW transition involving the C_2 symmetry breaking). This last assumption is necessary to guarantee that the crystal is identical when the C_2 rotation is applied even in a finite field. As shown in the top panel of Fig. 2(a), we assume a transverse electric field along the y axis (E_y^o) due to the in-plane Hall effect. We note that the experimental configuration is unchanged except for the direction of E_y^o , when we apply the C_2 rotation to the whole experimental setup including the B and the applied J (see the lower panel in Fig. 2(a)). This leads to the conclusion that $E_y^o = 0$, i.e., $\rho_{yx}^o = 0$. In the same way, we can prove the other conditions 2-4 in SI Sec. A.

Here, we apply the above symmetry conditions to selected examples to see if the in-plane Hall effect is allowed. Interesting contrast is obtained between the in-plane Hall effect in VS₂-VS-superlattice [34] and in ZrTe₅ [33]. As carefully discussed in Ref. [34], monoclinic unit cell allows the in-plane Hall effect, which is consistent with the experimental results. In the case of an orthorhombic point group mmm , however, it is indeed forbidden as long as the field is in one of the mirror planes, i.e., $\rho_{xy}^o(B_x, B_y, 0) = \rho_{yz}^o(0, B_y, B_z) = \rho_{zx}^o(B_x, 0, B_z) = 0$. Accordingly, the reported in-plane Hall effect ($\rho_{zx}(B_x, 0, B_z)$) in ZrTe₅ (space group: No. 63, $Cmcm$ at RT) [33] is forbidden by the ac mirror symmetry, where the xyz axes correspond to the crystallographic abc axes. The discrepancy between the symmetry condition and the experiments suggests an unrecognized symmetry lowering in the sample used, such as a monoclinic at low temperatures, or an unexpectedly large sensitivity to external shear strain or sample misalignment.

EFFECT OF LACK OF SYMMETRY 1: TWINS

As shown above, the in-plane Hall effect requires that the crystals lack certain symmetries. In real materials, this feature potentially causes twinning to cancel the signal expected in a monodomain. In practice, twinned crystals are avoided for measurements, but sometimes careful inspection miss a twin by merohedry [53], where its twin operation belongs to the holohedry point group (higher-symmetry group of the crystals). When the twin operation reverses the in-plane Hall voltage, the twin domains, crystal 1 and 2, contribute oppositely to the signal. If v is the volume ratio of the crystal 1, the total

in-plane Hall signal is

$$\rho_{yx}^{o,\text{tot}}(B_x, 0, 0) = v\rho_{yx}^{o,1} + (1-v)\rho_{yx}^{o,2} = (2v-1)\rho_{yx}^o, \quad (1)$$

which vanishes at $v = 0.5$. Similar situation occurs due to a twin by pseudo-merohedry [53] in a monoclinic crystal as shown in Fig. 3(a). Twinning due to a lack of mirror symmetry parallel to the xy plane results in the opposite contribution from each domain.

Another case is for a layered rhombohedral crystal, which potentially contains twinning by reticular merohedry (obverse-reverse twinning) [53]. We consider the crystal belonging to the point group $\bar{3}m$ (Fig. 3(b)). As the C_2 axis is absent along the x axis, the crystal often twinned with the domain associated with the C_2 rotation along the x axis (Fig. 3(c), top). Each domain contributes oppositely to the in-plane Hall signal along the y axis under B_x . This twinning occurs for example when there is the stacking fault regarding the inversion of ABC -stacked layers to CBA -stacked layers of triangular lattices (Fig. 3(c), bottom). To accurately evaluate the magnitude of the intrinsic in-plane Hall effect, we need to select de-twinned crystals, e.g., by checking crystallographic morphology or the extinction rules of the diffraction patterns.

EFFECT OF LACK OF SYMMETRY 2: OUT-OF-PLANE TRANSPORT

We consider a protocol for evaluating the intrinsic in-plane Hall conductivity for a twin-free crystal. We start by considering the relationship between conductivity and resistivity. A conductivity tensor ($\hat{\sigma}$) is a 3×3 matrix connecting an applied electric field (\mathbf{E}) and an induced current (\mathbf{J}):

$$\mathbf{J} = \hat{\sigma}\mathbf{E}. \quad (2)$$

Instead of measuring the conductivities directly, one usually attempts to measure resistivities because it is much easier to control the direction of the \mathbf{J} in a sample than to manage the \mathbf{E} . The resistivity tensor $\hat{\rho}$ connects the \mathbf{J} and \mathbf{E} inversely from the $\hat{\sigma}$:

$$\mathbf{E} = \hat{\rho}\mathbf{J} \quad (3)$$

As the theories usually provide the predictions of the conductivity, the accurate conversion of the experimental observation $\hat{\rho}$ to the $\hat{\sigma}$ is important to identify the underlying mechanisms of the in-plane Hall effect.

Here, we consider the following question. Suppose that we observe a non-zero $\rho_{yx}^o(B_x)$, can we immediately conclude that the signal is exclusively ascribed to the finite in-plane Hall conductivity (σ_{xy}^o)? It is, in fact, not the case because $\rho_{yx}^o(B_x)$ is contaminated with the effect of the out-of-plane transport in the three-dimensional system.

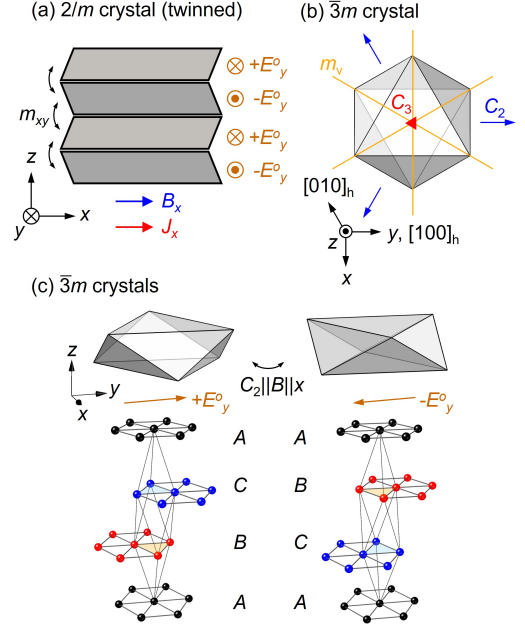


FIG. 3. (a) Twinning by pseudo merohedry in terms of m_{xy} for a $2/m$ crystal (the C_2 symmetry is along the y axis). Gray parallelograms are twin domains, where the in-plane Hall effect ($\propto E_y^o$) is opposite. (b) Schematic top-view of a trigonal crystal belonging to $\bar{3}m$ point group and symmetry elements. Red triangle: three-fold rotation along the z axis, C_3 . Blue arrows: in-plane two-fold rotations, C_2 , where one of them is along the y axis. There is no C_2 axis along the x axis. Orange lines: vertical mirror planes, m_v , one of which is parallel to the xz plane. Hexagonal axes ($[100]_h$ and $[010]_h$), and Cartesian coordinates, x , y , and z are also shown. (c) Two $\bar{3}m$ crystals with respect to the twinning by reticular merohedry (obverse-reverse twins), where the C_2 rotation along the x axis transforms one from the other. The induced in-plane Hall electric field E_y^o is reversed. The bottom panel shows a corresponding schematic rhombohedral ABC and CBA -stacking of triangular lattices, where a unit cell is emphasized by black lines.

We consider a monoclinic $2/m$ system (Fig. 4), which provides a typical formula of our interest with respect to the in-plane Hall conductivity. The conductivity tensor is as follows,

$$\hat{\sigma}_{2/m}(B_x) = \begin{pmatrix} \sigma_{xx}^e & \sigma_{xy}^o & \sigma_{xz}^e \\ -\sigma_{xy}^o & \sigma_{yy}^e & \sigma_{yz}^o \\ \sigma_{xz}^e & -\sigma_{yz}^o & \sigma_{zz}^e \end{pmatrix}. \quad (4)$$

Here, we set the C_2 axis parallel to the y axis and the mirror plane in the xz plane (Fig. 4). The z axis is defined as orthogonal to the xy plane. The superscripts, e and o, are for field-even and field-odd quantities, respectively. Since the tensor form of $\hat{\rho}$ is identical with that of $\hat{\sigma}$, we put

$$\hat{\rho}_{2/m}(B_x) = \begin{pmatrix} \rho_{xx}^e & -\rho_{yx}^o & \rho_{zx}^e \\ \rho_{yx}^o & \rho_{yy}^e & -\rho_{zy}^o \\ \rho_{zx}^e & \rho_{zy}^o & \rho_{zz}^e \end{pmatrix}. \quad (5)$$

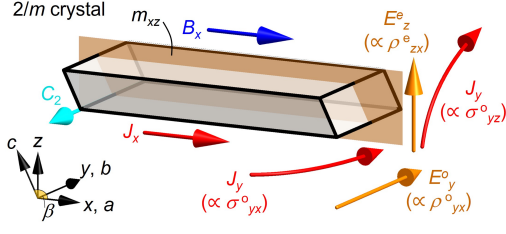


FIG. 4. Schematics of a $2/m$ crystal (gray parallelepiped) and the in-plane Hall effect. Orange plane is the mirror (m_{xz}) parallel to the xz plane. Cyan arrow is the C_2 axis along the y axis. xyz is the Cartesian coordinate introduced as $x \parallel a$ and $y \parallel b$, and β ($> 90^\circ$) is the angle between the a and c axes. The in-plane Hall effect E_y ($\propto \rho_{yx}^o$, oblique orange arrow) is allowed under $J \parallel B \parallel x$. The out-of-plane electric field E_z (vertical orange arrow) is induced by the crystalline planar Hall coefficient ($\propto \rho_{zx}^e J_x$). The out-of-plane current is deflected towards y by the Lorentz force from the B_x to induce J_y ($\propto \sigma_{yz}^o E_z$, red arrow on the right), which is added to the intrinsic J_y ($\propto \sigma_{yx}^o$, red arrow in the middle).

By taking the inverse matrix, $\hat{\rho} = \hat{\sigma}^{-1}$, we obtain the formula for ρ_{yx}^o :

$$\rho_{yx}^o = \frac{\sigma_{zz}^e}{\Delta_\sigma} (\sigma_{xy}^o + \sigma_{xz}^e \sigma_{yz}^o / \sigma_{zz}^e), \quad (6)$$

where Δ_σ is the determinant of $\hat{\sigma}$ (see SI Sec. B). We note that the ρ_{yx}^o is not directly proportional to the in-plane Hall conductivity σ_{xy}^o , but is contaminated by the term $\sigma_{xz}^e \sigma_{yz}^o / \sigma_{zz}^e$, where σ_{yz}^o corresponds to the Hall effect in the yz plane under B_x . This term is finite if the field-even component σ_{xz}^e is finite. We refer σ_{xz}^e (and ρ_{zx}^e) to the crystalline planar Hall effect (see SI Sec. C).

The contamination of the cross term between the σ_{yz}^o and σ_{xz}^e can be understood as shown in Fig. 4. The application of the current J_x generates the out-of-plane electric field E_z due to ρ_{zx}^e , which leads to the out-of-plane conduction J_z . In the presence of the B_x , the J_z is deflected in the yz plane to produce the transverse $J_y \propto \sigma_{yz}^o$, which produces an E_y together with the intrinsic in-plane Hall current ($J_y \propto \sigma_{yx}^o$) [54].

It is evident that in a monoclinic crystal the σ_{xz}^e can be finite even in zero field because $\beta \neq 90^\circ$ does not guarantee the diagonalized form of the conductivity tensor. As a matter of fact, the effect due to σ_{xz}^e is unavoidable for higher-symmetry systems when we consider the in-plane Hall effect of a three-dimensional system at finite field. We can prove that the symmetry condition for the finite in-plane Hall effect σ_{xy}^o is equivalent to that for the σ_{xz}^e (see SI Sec. C).

This contamination effect is serious if there is a significant anomalous (Berry curvature) contribution in σ_{yz}^o . We consider that Hall conductivity can be divided into two terms, normal (Lorentz force origin) and anomalous (Berry curvature origin) components, i.e., $\sigma_{xy}^o = \sigma_{xy}^N + \sigma_{xy}^A$ and $\sigma_{yz}^o = \sigma_{yz}^N + \sigma_{yz}^A$. The anomalous in-plane

Hall resistivity $\rho_{yx}^A(B_x)$ is, then, expressed as follows.

$$\rho_{yx}^A = \frac{\sigma_{zz}^e}{\Delta_\sigma} (\sigma_{xy}^A + \sigma_{xz}^e \sigma_{yz}^A / \sigma_{zz}^e). \quad (7)$$

Here, we omit the superscripts, e and o, for simplicity. Evidently, we cannot directly connect the observation of the ρ_{yx}^A with the presence of the σ_{xy}^A , and need to exclude the effect from σ_{yz}^A .

For quasi-two-dimensional systems, the situation is expected to become simpler. We assume that σ_{yz}^A is negligible. The yz components is small because we can prove that $\sigma_{yz}^N \propto \mu_z$, where μ_z is the out-of-plane carrier mobility. As the magnitude of σ_{xz}^e cannot exceeds $\sqrt{\sigma_{xx}^e \sigma_{zz}^e}$ (since $\Delta_\sigma > 0$), we can reasonably expect that the xz component is also restricted by the low μ_z ($\propto \sigma_{zz}^e$). These features can validate the assumption for ignoring the effect of the out-of-plane transport in the layered systems, and the approximation taking the resistivity and conductivity tensors as 2×2 matrices. In the next section, we consider the case of the quasi-two-dimensional system and how the σ_{xy}^o is measured.

EFFECT OF LACK OF SYMMETRY 3: ABSENCE OF xy -ROTATIONAL SYMMETRY.

In this section, we ignore the xz and yz components in $\hat{\sigma}$ and $\hat{\rho}$ (Eqs. (4), (5)) for the quasi-two-dimensional system. Even in such a simplified situation, we have to consider the absence of the xy -rotational symmetry.

To emphasize the distinction from the conventional normal Hall effect, we first consider the measurement of the isotropic system under a magnetic field along the z axis (Fig. 5(a)). A five-electrode measurement using a single-device is sufficient to estimate σ_{xy}^o , where two electrodes are connected to a current source, and three are used to monitor longitudinal and transverse voltage drops. We obtain $\rho_{xx}^e(B_z)$ ($= V_x / J_x \cdot wt / l_x$) and $\rho_{yx}^o(B_z)$ ($= V_y / J_x \cdot wt / l_y$), where l_x and l_y are the electrode distance for V_x and V_y , respectively. From the view-point of symmetry and Onsager's relation, we can put $\rho_{yy}^e(B_z) = \rho_{xx}^e(B_z)$ and $\rho_{xy}^o(B_z) = -\rho_{yx}^o(B_z)$. We obtain the single-device formula to estimate the normal Hall conductivity

$$\sigma_{xy}^o(B_z) = \rho_{yx}^o / [(\rho_{xx}^e)^2 + (\rho_{yx}^o)^2]. \quad (8)$$

In contrast to the above case, the σ_{xy}^o in the in-plane Hall system cannot be estimated within a single setup of the five-electrode measurement (Fig. 5(b)). The magnetoresistivity tensor when the magnetic field is applied along the x axis is given by

$$\hat{\rho}_{2D}(B_x) = \begin{pmatrix} \rho_{xx}^e & -\rho_{yx}^o \\ \rho_{yx}^o & \rho_{yy}^e \end{pmatrix}. \quad (9)$$

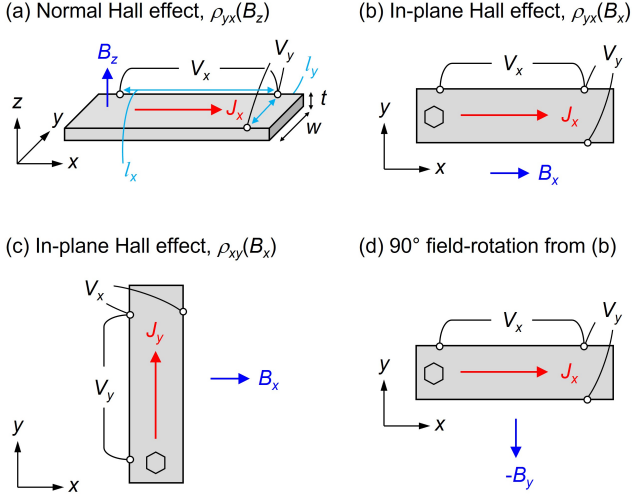


FIG. 5. Schematic five-electrode configurations for measurements of (a) a normal Hall effect, and (b) an in-plane Hall effect. The gray rectangle is a shaped sample with width w and thickness t . White circles are electrodes, and black lines are wires to measure longitudinal voltage drop V_x and transverse voltage difference V_y in an applied current along the x axis, J_x . The magnetic field is applied (a) perpendicular to the xy plane, B_z , and (b) along the x axis, B_x . In the setup of (b), we obtain $\rho_{xx}(B_x)$ and $\rho_{yx}(B_x)$. (c) is another setup for the in-plane Hall effect with J_y providing $\rho_{yy}(B_x)$ and $\rho_{xy}(B_x)$. (d) is the setup with 90° rotation of the magnetic field from (b), giving $\rho_{xx}(-B_y)$ and $\rho_{yx}(-B_y)$. A hexagon marker on each corner denotes the in-plane orientation of the sample (see text).

Here, we assume that the symmetry of the system is high enough to have the purely field-odd off-diagonal component, i.e., no planar Hall effect (this is not true, for example, for $\bar{3}$ and $\bar{3}$ systems [42]). Importantly, the inequality $\rho_{yy}^e(B_x) \neq \rho_{xx}^e(B_x)$ is unavoidable, in principle, because the in-plane magnetic field B_x always breaks the rotational symmetry around the z axis even in the case of the high-symmetric system in zero field (e.g., $\bar{3}m$, $3m$, and 32). The origin of the anisotropy can be easily understood because the longitudinal current ($J_x \parallel B_x$) is less affected by the Lorentz force than the transverse current ($J_y \perp B_x$). We also note that, in fact, the inequality $\rho_{xx}^e \neq \rho_{yy}^e$ often occurs in the in-plane Hall systems because it is mainly allowed in low-symmetric systems such as monoclinic crystals [11, 12, 34].

The inverse matrix of the resistivity tensor gives the longitudinal conductivity σ_{xx}^e as follows.

$$\begin{aligned} \sigma_{xx}^e(B_x) &= \rho_{yy}^e / [\rho_{xx}^e \rho_{yy}^e + (\rho_{yx}^e)^2] \\ &\sim \rho_{yy}^e / (\rho_{xx}^e \rho_{yy}^e) \sim 1 / \rho_{xx}^e \end{aligned} \quad (10)$$

Here, we assume in the last equality that the Hall angle ($\rho_{yx}^e / \rho_{xx}^e$) is negligible. We find that the longitudinal conductivity can be estimated with sufficient accuracy within a five-electrode measurement of the setup in Fig.

5(b). The Hall conductivity (σ_{xy}^o), on the other hand, is obtained in the exact form by using all three independent quantities, ρ_{xx}^e , ρ_{yy}^o , and ρ_{yx}^e (see SI Sec. B for the effect of three-dimensionality):

$$\sigma_{xy}^{o,\text{exact}}(B_x) = \rho_{yx}^o / [\rho_{xx}^e \rho_{yy}^e + (\rho_{yx}^e)^2] \sim \rho_{yx}^o / (\rho_{xx}^e \rho_{yy}^e). \quad (11)$$

To estimate $\rho_{yy}^e(B_x)$, we need to prepare another sample as shown in Fig. 5(c) with a long edge along the y axis and perform an experiment for J_y under B_x . We cannot measure $\rho_{yy}^e(B_x)$ with the same sample for the $J_x \parallel B_x$ (Fig. 5(b)) because it has to be shaped into a thin rectangular parallelepiped with a long edge along the x axis to increase the signal ($\propto l/wt$) as well as to suppress the geometrical effect [5, 55–57].

One might consider that we can measure $\rho_{xx}^e(-B_y)$ without changing the sample by rotating the magnetic field from B_x to $-B_y$ (Fig. 5(d)), which seems to be an alternative to $\rho_{yy}^e(B_x)$ in Eq. (9). This is in fact inapplicable because $\rho_{xx}^e(-B_y) \neq \rho_{yy}^e(B_x)$, which can be seen from the fact that a hexagon symbol on the sample in Fig. 5(d) changes its orientation when one tries to superimpose it on Fig. 5(c) by rotating the whole setup by -90° . The inequality $\rho_{xx}^e(-B_y) \neq \rho_{yy}^e(B_x)$ arises from the symmetry condition that forbids a C_{2z} symmetry for the non-zero in-plane Hall effect (see Fig. 2(c)), because this rule forbids C_{4z} symmetry at the same time. In other words, if there is a symmetry that ensures $\rho_{xx}^e(-B_y) = \rho_{yy}^e(B_x)$, one can prove $\rho_{yx}^o(B_x) = 0$, which is not the situation considered here.

Since the $\rho_{yy}^e(B_x)$ cannot be obtained within the single-device measurement using the setup in Fig. 5(b), the above formula is often replaced by the following approximate form:

$$\sigma_{xy}^{o,\text{approx}}(B_x) = \rho_{yx}^o / [(\rho_{xx}^e)^2 + (\rho_{yx}^e)^2] \sim \rho_{yx}^o / (\rho_{xx}^e)^2 \quad (12)$$

This prescription resembles Eq. (8) for the normal Hall effect, but contains a leap of logic implicitly assuming that $\rho_{xx}^e(B_x) = \rho_{yy}^e(B_x)$, which is in general invalid for the in-plane Hall system. Nevertheless, this approximate form of the Hall conductivity has often been used in many related experiments for orthorhombic/monoclinic compounds [34, 58–60], tilted-field configuration [37, 61, 62], xz -plane-transport of tetragonal systems [63], as well as for the in-plane thermal Hall conductivity in magnetic insulators [38, 39, 45].

Although this does not bring a big problem in many cases for the estimation of the order of magnitude, it is crucial when the accurate value of the (thermal) Hall conductivity is connected with the theoretical interpretation of the quantum nature of the material. In principle, we need to prepare two independent devices (Figs. 5(b)-(c)) and measure ρ_{xx}^e , ρ_{yy}^e , and ρ_{yx}^o , to apply Eq. (11) with all three independent components. In the next section, we discuss the in-plane thermal Hall effect in α -RuCl₃, where

the quantitative evaluation of the half-integer quantization has been concluded on the basis of the approximate form of κ_{xy}^o .

CASE OF THE HALF-INTEGER QUANTIZATION OF THERMAL HALL EFFECT IN α - RuCl_3

Evidently, all of the above arguments are applicable to the in-plane thermal Hall effect in insulators. In particular, an accurate evaluation of the thermal Hall conductivity is important as argued in recent studies on the half-integer quantization of κ_{xy} under an in-plane and a tilted magnetic field in a Kitaev spin-liquid candidate α - RuCl_3 [37, 38, 64–66].

The crystal structure of α - RuCl_3 consists of a stacked honeycomb-lattice of Ru^{3+} with magnetic moments (Fig. 6). There are two orthogonal axes in the lattice plane, which are called zigzag (x axis) and armchair (y axis) directions, perpendicular and parallel to a Ru-Ru bond, respectively. α - RuCl_3 is antiferromagnetically ordered at below 7 K, and an in-plane magnetic field of 7 T is required to suppress the ordered state [37].

The half-integer quantization of the thermal Hall conductivity is observed in the field-induced spin-disordered state when the heat current is applied along the zigzag direction (x axis) and the magnetic field is applied along the same direction or tilted from the axis perpendicular to the honeycomb-lattice plane (z axis) towards the x axis [37, 38, 64–66]. The in-plane Hall effect in a honeycomb layer is allowed by symmetry [49], and the absence of thermal Hall effect in the magnetic field along the armchair direction (y axis) [38] follows the symmetry condition of honeycomb-lattice of edge-shared RuCl_6 octahedra [49]. The κ_{xy} is normalized to each honeycomb-lattice with the layer separation by d : $\kappa_{xy}^{2D}/T = \kappa_{xy} \cdot d/T$, which shows a quantization to the half value of $K_0 = (\pi^2 k_B^2/3h)T$, implying the presence of the edge current of Majorana fermions [36, 67].

Indeed, the access to the spin-disordered state requires the in-plane component of the magnetic field, which breaks the xy -plane rotational symmetry regardless of the crystal structure at low temperature. The exact form of the in-plane thermal Hall conductivity is expressed by

$$\kappa_{xy}^{o,\text{exact}}(B_x) \sim \lambda_{yx}^o / \lambda_{xx}^e \lambda_{yy}^e, \quad (13)$$

and it requires all the three independent thermal resistivity components, $\lambda_{xx}^e(B_x)$, $\lambda_{yy}^e(B_x)$, and $\lambda_{yx}^o(B_x)$ (we can reasonably ignore the effect of the out-of-plane transport; see below). In previous studies, however, the thermal Hall conductivity has been estimated by the approximate form [37, 39, 65, 66, 68, 69]:

$$\kappa_{xy}^{o,\text{approx}}(B_x) \sim \lambda_{yx}^o / (\lambda_{xx}^e)^2, \quad (14)$$

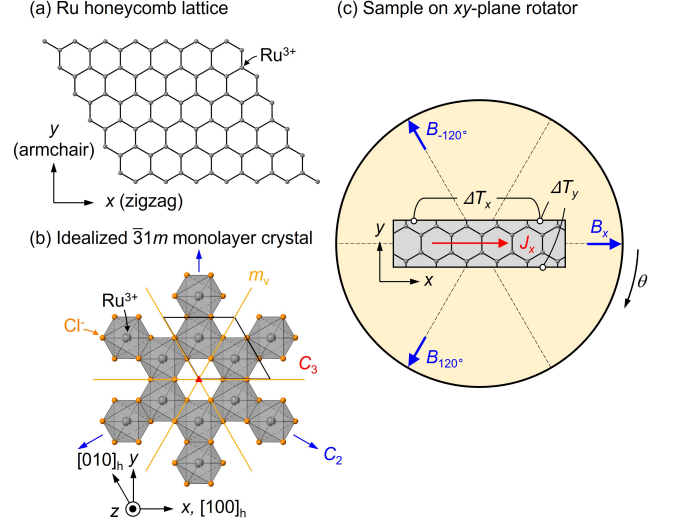


FIG. 6. (a) Schematic honeycomb lattice of Ru^{3+} ions. Zigzag ($\parallel x$) and armchair ($\parallel y$) axes are defined. (b) The idealized honeycomb layer of α - RuCl_3 belonging to the point group $\bar{3}1m$. Hexagonal axes, Cartesian coordinates, x , y , and z , the unit cell (black rhombus), and symmetry elements are also shown (see Fig. 3(b)). (c) Schematic improved single-device setup for the in-plane thermal Hall effect of α - RuCl_3 under the in-plane magnetic field along x axis (B_x), and directions rotated by $\pm 120^\circ$ around the z axis ($B_{\pm 120^\circ}$). The electrodes are for the measurement of longitudinal (ΔT_x) and transverse (ΔT_y) temperature differences.

where the equivalence $\lambda_{xx}^e(B_x) = \lambda_{yy}^e(B_x)$ is implicitly assumed.

To the best of our knowledge, the component $\lambda_{yy}^e(B_x)$ has scarcely been reported, i.e., the thermal conductivity with heat current along the armchair direction (y axis) under a field along the zigzag direction (x axis), except for Ref. [70]. We summarize the references that report the thermal transport properties of α - RuCl_3 and experimental conditions in SI Sec. D. The thermal Hall experiment with J_y under B_x is missing. As discussed in the above sections, we note that the $\lambda_{yy}^e(B_x)$ cannot be replaced by $\lambda_{xx}^e(-B_y)$, which is realized by rotating the in-plane field from B_x to B_y without changing the sample setup for $J \parallel x$. It is also known from the experimental results giving the different magnetic phase diagrams for B_x and B_y [64, 71]. Reference [70] reports both $\lambda_{xx}^e(B_x)$ and $\lambda_{yy}^e(B_x)$ (but no $\lambda_{yx}^o(B_x)$) with different samples. They show similar B_x -field dependence but their magnitudes are discernibly different, implying the possible anisotropy between $\lambda_{xx}^e(B_x)$ and $\lambda_{yy}^e(B_x)$.

Although the significant κ_{xy}^o in α - RuCl_3 has been repeatedly observed and the plateau feature has been reproduced [37, 64–66], there are still debates in terms of the accurate value in the spin-disordered region [39, 40], and microscopic origins of the κ_{xy}^o [39, 40, 72–74]. As the theoretical predictions are provided by the κ_{xy}^o , the ac-

curate conversion process from the experimentally measured thermal resistivity $\hat{\lambda}$ to the thermal conductivity $\hat{\kappa}$ is important. The controversy is potentially due to the estimation of κ_{xy}^o by the application of the approximate form Eq. (14), which may be sensitive to the sample dependence of anisotropy between λ_{xx}^e and λ_{yy}^e . For a more quantitative verification of the half-integer quantization, an experimental proof of the hypothesis $\lambda_{yy}^e(B_x) \simeq \lambda_{xx}^e(B_x)$ in the spin-disordered field region has to be provided at least within the precision of better than 10% comparable to that of the geometric errors [38]. A practical difficulty would arise from the notorious sample dependence [64, 65], which would obscure the possible equivalence between $\lambda_{yy}^e(B_x)$ and $\lambda_{xx}^e(B_x)$. We discuss two experimental protocols that take into account the sample quality variations and can be applied to α -RuCl₃ to quantitatively verify the half-integer value of κ_{xy} .

One of the approaches is to make use of the three-fold rotational symmetry, which is supposed to be realized in the low-temperature crystal structure of α -RuCl₃ [75, 76], although it seems to be still under discussion [69, 77–79]. The advantage of this method is that it can directly measure the anisotropy of the thermal resistivity $\lambda_{xx}^e - \lambda_{yy}^e$ under the magnetic field without changing the sample (improved single-device method). The idea is similar to the method proposed in Refs. [80 and 81], where the elasto-resistive effect is considered.

Here, we assume that the crystal structure of a monolayer α -RuCl₃ effectively belongs to the $\bar{3}1m$ point group, as shown in Fig. 6(b). There are three two-fold rotation axes and three vertical mirrors, which are related to each other by three-fold rotational symmetry. We note that the proposed space group $R\bar{3}$ at low temperature [76, 82, 83] is expected to make the tensor components more complicated [42, 49] due to the ferroaxial nature of the point group [84, 85]. The absence of $\kappa_{xy}(B_y)$ in α -RuCl₃ [38], which is allowed in the $\bar{3}$ system, validates this setting. According to the symmetry conditions for the in-plane thermal Hall effect, the form of $\hat{\lambda}$ is obtained from Eq. (9) by replacing ρ with λ .

First, we prepare a sample for the measurement with J_x and B_x (Fig. 6(c)). We obtain the field dependence of $\lambda_{xx}^e(B_x)$ ($\propto \Delta T_x$), and $\lambda_{yx}^o(B_x)$ ($\propto \Delta T_y$ with the antisymmetrization by field), but not $\lambda_{yy}^e(B_x)$. Instead, we measure the anisotropy $\lambda_{xx}^e - \lambda_{yy}^e$ by rotating the magnetic field *in-situ* around the z axis by 120° and perform the same measurement (see left bottom of Fig. 6(c)). This configuration is similar to the planar Hall effect measurement, and the presence of the field-even off-diagonal component can be known, that is in fact proportional to $\lambda_{xx}^e - \lambda_{yy}^e$.

Due to the three-fold rotational symmetry of the crystal, we can accurately predict the form of $\hat{\lambda}(B_{120^\circ})$ using

Eq. (6) with the rotation matrix, \mathcal{R}_{120° ,

$$\begin{aligned} \hat{\lambda}_{2D}(B_{120^\circ}) &= \mathcal{R}_{120^\circ}^{-1} \hat{\lambda}_{2D}(B_x) \mathcal{R}_{120^\circ} \\ &= \begin{pmatrix} (\lambda_{xx}^e + 3\lambda_{yy}^e)/4 & -\lambda_{yx}^o + \sqrt{3}(\lambda_{xx}^e - \lambda_{yy}^e)/4 \\ \lambda_{yx}^o + \sqrt{3}(\lambda_{xx}^e - \lambda_{yy}^e)/4 & (3\lambda_{xx}^e + \lambda_{yy}^e)/4 \end{pmatrix} \end{aligned} \quad (15)$$

Accordingly, we obtain $\lambda_{yx}^o + \sqrt{3}(\lambda_{xx}^e - \lambda_{yy}^e)/4$ as the off-diagonal component. By measuring the field-dependence, we separate the field-symmetric and antisymmetric components in the yx component, respectively, as

$$\lambda_{yx}^S(B_{120^\circ}) = \sqrt{3}(\lambda_{xx}^e - \lambda_{yy}^e)/4 + \delta \quad (16)$$

and

$$\lambda_{yx}^{AS}(B_{120^\circ}) = \lambda_{yx}^o. \quad (17)$$

We introduce the δ term in the first equation, which is proportional to the longitudinal component owing to the possible misalignment of the Hall electrodes.

The δ term can be eliminated by performing the same measurement with the field rotation by -120° (left top of Fig. 6(c)). The field-symmetric contribution to the off-diagonal thermal Hall resistivity is given as

$$\lambda_{yx}^S(B_{-120^\circ}) = -\sqrt{3}(\lambda_{xx}^e - \lambda_{yy}^e)/4 + \delta. \quad (18)$$

We note that the intrinsic component ($\propto \lambda_{xx}^e - \lambda_{yy}^e$) is reversed from that for B_{120° , while the extrinsic δ term is not. An antisymmetrization with respect to $\pm 120^\circ$ can be defined as $\lambda_{yx}^{S'}(|B|) = (\lambda_{yx}^e(B_{120^\circ}) - \lambda_{yx}^e(B_{-120^\circ}))/2$. We obtain $\lambda_{yx}^{S'} = \sqrt{3}(\lambda_{xx}^e - \lambda_{yy}^e)/4$, which provides the anisotropy between $\lambda_{xx}^e(B_x)$ and $\lambda_{yy}^e(B_x)$. Here, we note that the field dependence of λ_{xx}^e , λ_{yy}^e , and λ_{yx}^o in each equation are identical to those of B_x due to the three-fold rotational symmetry unless the demagnetization effect is significant.

The measurement can be done within a single-device by using an appropriate sample stage with rotators. The demonstration of $\lambda_{yx}^{S'} = 0$ gives a proof for $\lambda_{xx}^e(B_x) = \lambda_{yy}^e(B_x)$, which justifies the approximate form of Eq. (14) for estimating the thermal Hall conductivity in α -RuCl₃. Otherwise, the exact form of Eq. (13) has to be used to accurately estimate κ_{xy}^o in the spin-disordered regime, suggesting the need for a correction of the reported half-integer value.

The other approach to verify $\lambda_{xx}^e = \lambda_{yy}^e$ in α -RuCl₃ is to measure two different samples (two-device method), and to utilize the thermal Hall effect itself as a sample quality check. This can be done by preparing two high-quality samples that show quantized $\kappa_{xy}^{o, \text{approx}}/T = \frac{1}{2}K_0/d$ in individual setups for the heat current parallel to the x and y axis (Figs. 5(b) and 5(c)), respectively. For a sample in the J_x setup (sample X), we measure

$$\kappa_{xy}^{X, \text{approx}}(B_x) = \lambda_{yx}^X / (\lambda_{xx}^X)^2. \quad (19)$$

With a sample in the J_y setup (sample Y), we obtain

$$\kappa_{y(-x)}^{Y,\text{approx}}(B_x) = \lambda_{(-x)y}^Y / (\lambda_{yy}^Y)^2. \quad (20)$$

Here, we omit e and o for simplicity.

If we find that the thermal Hall plateaus are quantized to $\kappa_{xy}^{X,\text{approx}}(B_x, T)d/T \simeq \kappa_{y(-x)}^{Y,\text{approx}}(B_x, T)d/T \simeq \frac{1}{2}K_0$, we can confirm their comparable quality. And, we obtain an indirect proof of $\lambda_{yy}^e(B_x, T) \simeq \lambda_{xx}^e(B_x, T)$ because

$$1 \simeq \sqrt{\kappa_{xy}^{X,\text{approx}}(B_x, T) / \kappa_{y(-x)}^{Y,\text{approx}}(B_x, T)} = \lambda_{yy}^Y / \lambda_{xx}^X. \quad (21)$$

On the other hand, if the reproducibility of a different quantization $\kappa_{y(-x)}^{Y,\text{approx}}(B_x)d/T = rK_0$ ($r \neq \frac{1}{2}$) is established for the J_y setup, it may be an artifact due to the approximate forms of the κ_{xy} (Eq. (14)), and the precise thermal Hall conductivity could be estimated by a geometric mean

$$\kappa_{xy}^{\text{exact}}d/T \simeq \sqrt{\kappa_{xy}^{X,\text{approx}}\kappa_{xy}^{Y,\text{approx}}}d/T = \sqrt{r/2}K_0 \neq \frac{1}{2}K_0. \quad (22)$$

This would provide an opportunity to reconsider the true quantization value of the thermal Hall conductivity in α -RuCl₃.

The preceding discussion is about the effect due to the possible anisotropy between $\lambda_{xx}^e(B_x)$ and $\lambda_{yy}^e(B_x)$. For the quantitative evaluation of the κ_{xy} in α -RuCl₃, two additional effects mentioned above also have to be considered. For the proposed space group $R\bar{3}$ at low temperature, there are twin operations that change the orientation of the RuCl₆ octahedra and reverse the sign of $\kappa_{xy}(B_x)$: the C_2 operation perpendicular to the honeycomb lattice (C_{2z}) and the mirror operation m_{yz} . It has been pointed out that the $ABAB$ -stacking of the honeycomb-layers in the ABC -stacking affects the magnetic transition temperature [69, 79, 86, 87], and such crystals can be avoided by the magnetization measurements [37, 38]. Since the twin domains due to the C_{2z} and m_{yz} are expected to have the same transition temperature, the twinned crystals can only be distinguished, for example, by checking the intensity profile of the electron/x-ray diffraction pattern (see SI Sec. D). As for the out-of-plane thermal transport, it has been reported [88] to be comparable to the in-plane transport, while the out-of-plane thermal Hall effect λ_{yz}^o (and also λ_{xz}^e) has not been reported. Nevertheless, this effect may be negligible as the thermal Hall angle $\lambda_{yz}^o/\lambda_{zz}^e$ is expected to be significantly small in magnetic insulators [89].

CONCLUSION.

Unlike the normal Hall effect, the in-plane (thermal) Hall effect is a response where the lack of crystal symmetry is essential. As a result, several factors, including

crystal twinning, out-of-plane transport, and in-plane rotational symmetry, have to be taken into account in order to quantitatively evaluate the Hall conductivity under the in-plane field condition. To accurately extract the Hall conductivity from the measured resistivity components, a formalism beyond the conventionally-used formula is required because the xy -plane symmetry is inevitably broken.

In principle, two independent experimental setups are required to measure at least three independent components in the (thermal) resistivity tensor (two-device method). Possible sample dependence may prevent an accurate conversion to the conductivity tensors, while the values of the Hall resistivity in individual experiments can be used as a check of the equivalence of the sample quality. Another improved single-device approach using the rotation of the in-plane field is possibly available when the crystal has three-fold rotational symmetry, which is the archetype of the in-plane Hall system for the theoretical consideration of the quantized anomalous Hall effect [19–23, 25, 33], and thermal Hall effect of Kitaev-related honeycomb magnets [49, 72–74]. The protocols presented in this manuscript would be useful to shed additional light on the experimental evidence for the quantization of κ_{xy} in α -RuCl₃, and more generally applicable to the evaluation of the unconventional in-plane Hall conductivity of a broader class of quantum materials.

ACKNOWLEDGMENT

T.K. was financially supported by Ministry of Education Culture Sports Science and Technology (MEXT) Leading Initiative for Excellent Young Researchers (JPMXS0320200135), Japan Society for the Promotion of Science (JSPS) KAKENHI Grant-in-Aid for Young Scientists B (No. 21K13874). We thank L. Ye, T.-h. Arima, J. G. Checkelsky, and S. Kitou for fruitful discussion and comments on the manuscript.

SUPPLEMENTARY MATERIALS

**A. LIST OF POINT GROUPS FOR THE
NON-ZERO IN-PLANE HALL EFFECT**

In the main text, we show that the in-plane Hall effect is allowed only when some symmetries are absent. As an example, we prove that the two-fold rotation axis along the magnetic field is forbidden (Condition 1, see Fig. 2(a)). The proofs for the Conditions 2 to 4 (Fig. 2(b)-(c)) are given as follows.

We can apply the corresponding logic to the system with a mirror symmetry perpendicular to the magnetic field (Condition 2, Fig. 2(b)). The orientation of J_x is reversed by the m_{yz} while the sample configuration (including the induced para- or diamagnetic moment), E_y^o , and B_x remain the same. This relationship gives the equation

$$E_y^o = \rho_{yx}^o(B_x, 0, 0) \cdot J_x = \rho_{yx}^o(B_x, 0, 0) \cdot (-J_x), \quad (\text{S1})$$

proving that $\rho_{yx}^o = 0$.

As for the two-fold rotational axis along the z axis (Condition 3, see Fig. 2(c)), we can prove the absence of the in-plane Hall effect. This is the case when the crystal has C_2 , C_4 , S_4 , or C_6 rotational symmetry along the z axis in zero field. We assume that although the magnetic field induces para- or diamagnetic moments in the xy plane, they do not reduce the symmetry of the system lower than $\mathcal{T}C_{2z}$, where \mathcal{T} is the time reversal operation. The C_{2z} rotation of the whole setup changes the upper panel to the bottom in Fig. 2(c). We obtain the following equations

$$E_y^o = \rho_{yx}^o(B_x, B_y, 0) \cdot J_x, \quad (\text{S2})$$

$$-E_y^o = \rho_{yx}^o(-B_x, 0, 0) \cdot (-J_x). \quad (\text{S3})$$

Since $\rho_{yx}^o(-B_x, 0, 0) = -\rho_{yx}^o(B_x, 0, 0)$, we prove that $\rho_{yx}^o = 0$.

For the mirror symmetry in the xy plane (Condition 4, see Fig. 2(d)), the proof is as follows. Again, we note that the system becomes symmetric against $\mathcal{T}m_{xy}$ operation under the in-plane magnetic field. The equation for the upper panel in Fig. 2(d) is $E_y^o = \rho_{yx}^o(B_x, B_y, 0) \cdot J_x$, and the mirror operation to the experimental setup gives $E_y^o = \rho_{yx}^o(-B_x, -B_y, 0) \cdot J_x$. The last equation gives $-E_y^o = \rho_{yx}^o(B_x, B_y, 0) \cdot J_x$ to prove $\rho_{yx}^o = 0$.

On the basis of the Conditions 1 to 4, we produce the list of the crystal point groups that allow the in-plane Hall effect. Table I summarizes such point groups and allowed $\hat{\rho}$ components and field-configurations required to induce the in-plane Hall. The leading term with respect to the applied field is also shown. The absence of the orthorhombic point groups in the table indicates that they do not allow the in-plane Hall effect as long as the

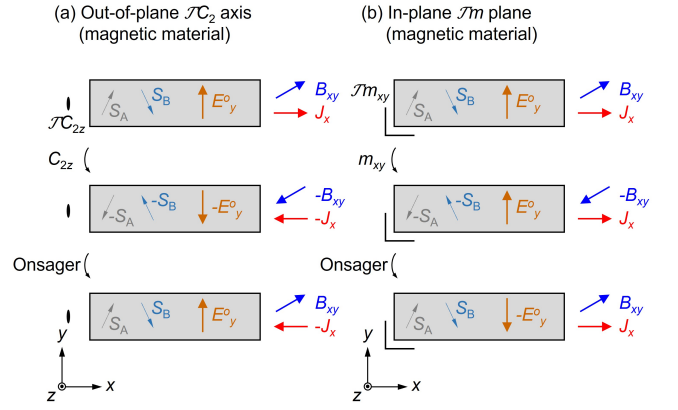


FIG. S1. Symmetry conditions 3' and 4' for the absence of the in-plane Hall effect in magnetic materials. See the caption of Fig. 2 for details. The gray and pale blue arrows in the crystal represent the ordered magnetic moments, S_A and S_B , which are canted by the applied magnetic field. (a) Application of the C_{2z} rotation to the whole setup including the crystal with $\mathcal{T}C_{2z}$ symmetry transforms the top to the middle, which is accompanied with the inversion of E_y^o , B_{xy} , and J_x . The Onsager's relation (Eq. (S4)) allows the transformation from the middle to the bottom. (b) Corresponding figure for the crystal with $\mathcal{T}m_{xy}$ symmetry.

applied field is in the high-symmetry directions such as the xy plane.

In the same table, we show the symmetry conditions for the in-plane Hall effect in the magnetic materials, where the time-reversal symmetry is broken due to internal magnetic order parameters. The low-field expansion of the Hall coefficient for all magnetic point groups has been given in Ref. [43], which gives the allowed Hall coefficients up to the B -linear term. We present the extension to the arbitrary field region. Evidently, we can apply the same discussion to the two cases (systems with the symmetry C_{2x} , or m_{yz} , Condition 1' and 2', corresponding to Figs. 2(a)-(b)) considered in the main text to derive the $\rho_{yx}^o(B_x)$ even for magnetic materials. We also have to assume that the B_x does not induce the further symmetry breaking that lowers the C_{2x} or m_{yz} symmetry, which would be reasonably satisfied in many materials such as ferromagnets with magnetization $M \parallel x$ and two-sublattice antiferromagnets with sublattice moments $S_{A/B} \parallel x$. For the antiferromagnets with $S_{A/B} \parallel y$ or z or more complicated noncolinear magnets, we have to carefully check if the spin canting due to B_x does not lower the original symmetries.

In addition to the above, there are the other six symmetries need to be considered, i.e., $\mathcal{T}C_2$ along the z axis (Condition 3'), $\mathcal{T}m$ in the xy plane (Condition 4'), C_2 along the z axis (Condition 5'), m in the xy plane (Condition 6'), $\mathcal{T}C_2$ along the x axis (Condition 7'), and $\mathcal{T}m$ in the yz plane (Condition 8'). We separate them into three parts, and show the pictorial approaches to prove

TABLE I. Symmetry conditions for the non-zero in-plane Hall effect. The superscript o is omitted for simplicity. Point groups that allow the anomalous Hall effect are marked with an asterisk.

Point group	Symmetry axes	Allowed in-plane Hall effect	Leading term ($\propto B^n$)
Para- or diamagnetic materials			
1, $\bar{1}$	arbitrary xyz setting	$\rho_{yx}(B_x, B_y, 0)$	$\propto B$
2, m , $2/m$	$C_2 \parallel y$ or $m \parallel xz$	$\rho_{yx}(B_x), \rho_{yz}(B_z)$	$\propto B$
4, $\bar{4}$, $4/m$	C_4 or $S_4 \parallel z$	$\rho_{xz}(B_x), \rho_{yz}(B_y)$	$\propto B$
3, $\bar{3}$	$C_3 \parallel z$	$\rho_{xy}(B_x, B_y, 0), \rho_{xz}(B_x), \rho_{yz}(B_y)$	$\propto B$ for ρ_{xz}/yz $\propto B^3$ for ρ_{xy}
32, $3m$, $\bar{3}m$	$C_3 \parallel z, C_2 \parallel y$ or $m \parallel xz$	$\rho_{xy}(B_x)$	$\propto B^3$
6, $\bar{6}$, $6/m$	C_6 or $S_3 \parallel z$	$\rho_{xz}(B_x), \rho_{yz}(B_y)$	$\propto B$
23, $m\bar{3}$	$C_3 \parallel [111] \parallel z$	$\rho_{xy}(B_x, B_y, 0), \rho_{xz}(B_x), \rho_{yz}(B_y)$	$\propto B$ for ρ_{xz}/yz $\propto B^3$ for ρ_{xy}
432, $\bar{4}3m$, $m\bar{3}m$	$C_3 \parallel [111] \parallel z, C_2 \parallel [1\bar{1}0] \parallel y$ or $m \perp [1\bar{1}0]$	$\rho_{xy}(B_x)$	$\propto B^3$
Magnetic materials			
1*, $\bar{1}^*$, $\bar{1}'$	arbitrary xyz setting	$\rho_{yx}(B_x, B_y, 0)$	$\propto B$
2*, m^* , $2/m^*$	$C_2 \parallel y$ or $m \parallel xz$	$\rho_{yx}(B_x), \rho_{yz}(B_z)$	$\propto B$
2'*, m'^* , $2'/m'^*$	$\mathcal{T}C_2 \parallel y$ or $\mathcal{T}m \parallel xz$	$\rho_{yx}(B_x), \rho_{yz}(B_z)$	$\propto B$
2/m', $2'/m$	$(\mathcal{T})C_2 \parallel y$ or $(\mathcal{T})m \parallel xz$	$\rho_{yx}(B_x), \rho_{yz}(B_z)$	$\propto B$
4*, $\bar{4}^*$, $4/m^*$	C_4 or $S_4 \parallel z$	$\rho_{xz}(B_x), \rho_{yz}(B_y)$	$\propto B$
4', $\bar{4}'$, $4'/m$	$\mathcal{T}C_4$ or $\mathcal{T}S_4 \parallel z$	$\rho_{xz}(B_x), \rho_{yz}(B_y)$	$\propto B$
4/m', $\bar{4}'/m'$	C_4 or $\mathcal{T}S_4 \parallel z$	$\rho_{xz}(B_x), \rho_{yz}(B_y)$	$\propto B$
3*, $\bar{3}^*$, $\bar{3}'$	$C_3 \parallel z$	$\rho_{xy}(B_x, B_y, 0), \rho_{xz}(B_x), \rho_{yz}(B_y)$	$\propto B$ for ρ_{xz}/yz $\propto B^3$ for ρ_{xy}
32, $3m$, $\bar{3}m$	$C_3 \parallel z, C_2 \parallel y$ or $m \parallel xz$	$\rho_{xy}(B_x)$	$\propto B^3$
32'*, $3m'^*$, $\bar{3}m'^*$	$C_3 \parallel z, \mathcal{T}C_2 \parallel y$ or $\mathcal{T}m \parallel xz$	$\rho_{xy}(B_x)$	$\propto B^3$
$\bar{3}'m'$, $\bar{3}'m$	$C_3 \parallel z, \mathcal{T}C_2 \parallel y$ or $\mathcal{T}m \parallel xz$	$\rho_{xy}(B_x)$	$\propto B^3$
6*, $\bar{6}^*$, $6/m^*$	C_6 or $S_3 \parallel z$	$\rho_{xz}(B_x), \rho_{yz}(B_y)$	$\propto B$
6', $\bar{6}'$, $6'/m'$	$\mathcal{T}C_6$ or $\mathcal{T}S_3 \parallel z$	$\rho_{xz}(B_x), \rho_{yz}(B_y)$	$\propto B$
6/m', $\bar{6}'/m$	C_6 or $\mathcal{T}S_3 \parallel z$	$\rho_{xz}(B_x), \rho_{yz}(B_y)$	$\propto B$
23, $m\bar{3}$, $m'\bar{3}$	$C_3 \parallel [111] \parallel z$	$\rho_{xy}(B_x, B_y, 0), \rho_{xz}(B_x), \rho_{yz}(B_y)$	$\propto B$ for ρ_{xz}/yz $\propto B^3$ for ρ_{xy}
432, $\bar{4}3m$, $m\bar{3}m$	$C_3 \parallel [111] \parallel z, C_2 \parallel [1\bar{1}0] \parallel y$ or $m \perp [1\bar{1}0]$	$\rho_{xy}(B_x)$	$\propto B^3$
4'32, $\bar{4}'3m'$, $m\bar{3}m'$	$C_3 \parallel [111] \parallel z, C_2 \parallel [1\bar{1}0] \parallel y$ or $\mathcal{T}m \perp [1\bar{1}0]$	$\rho_{xy}(B_x)$	$\propto B^3$
$m'\bar{3}m'$, $m'\bar{3}m$	$C_3 \parallel [111] \parallel z, C_2 \parallel [1\bar{1}0] \parallel y$ or $\mathcal{T}m \perp [1\bar{1}0]$	$\rho_{xy}(B_x)$	$\propto B^3$

that they give the absence of the in-plane Hall effect.

First, we consider the following two symmetry conditions: $\mathcal{T}C_2$ along the z axis, and $\mathcal{T}m$ in the xy plane on the basis of Figs. S1(a)-(b).

3' $\rho_{yx}^o(B_x, B_y, 0)$ is zero if there is a $\mathcal{T}C_2$ axis along the z direction under the magnetic field.

We can prove this in three steps. First, we consider the magnetic material with $\mathcal{T}C_{2z}$ symmetry under a magnetic field along the x axis. Figure S1(a) shows the schematic in-plane field configuration, where we symbolically introduce the internal magnetic moments, S_A and S_B , which represent the internal time-reversal symmetry breaking [90]. In the top panel, we assume that the in-plane Hall electric field E_y is induced by the J_x . We apply the pure two-fold rotation to the whole setup to obtain the middle panel. We note that the internal magnetic moments are all reversed since $C_{2z} = \mathcal{T}^{-1}$ for the $\mathcal{T}C_{2z}$ -symmetric system. The internal mag-

netic moments can be reversed by the Onsager's relation (see Ref. [43] for detail)

$$\begin{aligned} \rho_{yx}^o(-S_A, -S_B, -\mathbf{B}) &= \rho_{yx}^o(S_A, S_B, \mathbf{B}) \\ &= -\rho_{yx}^o(S_A, S_B, \mathbf{B}). \end{aligned} \quad (\text{S4})$$

The last equation can be expressed by the bottom panel in Fig. S1(a). Comparing the top and the bottom, we find that E_y^o does not change its sign even if we reverse the current direction, which gives the proof for $\rho_{yx}^o = 0$.

4' $\rho_{yx}^o(B_x, B_y, 0)$ is zero if there is a $\mathcal{T}m$ in the xy plane under the magnetic field.

We can apply the same discussion for the above. Application of the pure m_{xy} operation to the whole setup reverses the magnetic field direction in the xy plane as well as the internal magnetic moments (top to middle in Fig. S1(b)). The Onsager's relation gives the transformation from the middle panel to

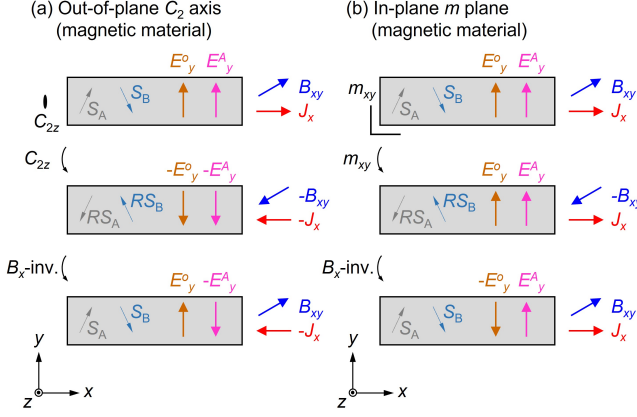


FIG. S2. Symmetry conditions 5' and 6' for the absence of the in-plane Hall effect in magnetic materials. See the caption of Figs. 2 and S1 for details. The magnetic order parameters, S_A and S_B , potentially have the out-of-plane component to induce magnetization along the z axis for the anomalous Hall system. The magnetic moments are canted by the applied magnetic field to break the zero-field symmetry. For the case of the anomalous Hall system, pink arrows indicate the electric field due to the anomalous Hall effect, E_y^A under $\pm J_x$. We put the B_{xy} -field-odd transverse electric field E_y^o as a tentative in-plane Hall effect, which is proved to be zero. (a) The case for the crystal with the C_{2z} rotational symmetry in zero field. Application of the C_{2z} rotation to the whole setup transforms the top to the middle, which is accompanied with the inversion of E_y^o , E_y^A , B_{xy} , and J_x . The magnetic moments are rotated to $\mathcal{R}S_{A/B}$. The B_{xy} -field inversion induces the transformation from the middle to the bottom. (b) Corresponding figure for the crystal with the m_{xy} as the zero-field symmetry.

the bottom panel, which gives the opposite sign of E_y^o from the top, i.e., $\rho_{yx}^o = 0$.

Next, we consider the other two cases: systems with symmetries C_{2z} or m_{xy} in zero field. In contrast to the nonmagnetic cases (Figs. 2(c)-(d)), the C_{2z} and m_{xy} symmetries are potentially accompanied by the anomalous Hall effect ρ_{yx}^A unless additional symmetries forbid the out-of-plane magnetization [43]. Strictly, the application of the B_{xy} field breaks the symmetry C_{2z} or m_{xy} due to canting of magnetic moments, nevertheless, we can prove that the B_{xy} -field induced Hall effect to be zero. This means that we can even observe the Hall voltage under the in-plane field in such systems, but it cannot be viewed as the intrinsic in-plane Hall effect, but the field-evolution of the anomalous Hall effect $\rho_{yx}^A(B_{xy})$. Sign of $\rho_{yx}(B_{xy})$ only depends on the sign of the order parameters (regarding S_A and S_B) responsible for the anomalous Hall effect, i.e., its field dependence is symmetric with respect to the B_{xy} unless the out-of-plane magnetization is flipped.

To prove the above in the pictorial approach, we consider below.

5' $\rho_{yx}^o(B_x, B_y, 0)$ is zero if there is a C_2 along the z axis in zero field unless the applied field flips the spontaneous magnetization.

As shown by the top panel in Fig. S2(a), we consider whether E_y^o is zero in the magnetic material under J_x . Due to the applied B_{xy} , the internal magnetic moments are canted to break the zero-field C_{2z} symmetry. Here, since the B in the exact xy plane does not lift the degeneracy for the out-of-plane magnetization, we consider the magnetic monodomain state and assume that the possible anomalous Hall electric field E_y^A is maintained to be the same sign even if the B_{xy} is swept from positive to negative. We apply the C_{2z} rotation to the whole system to obtain the middle panel, where the internal moments are also rotated to $\mathcal{R}S_{A/B}$ symbolically. The B_{xy} -field inversion transforms the middle to the bottom, where E_y^o is reversed by definition. We can safely assume that the internal moments rotate back to $S_{A/B}$ keeping the sign of E_y^A as the exact B_{xy} field does not flip the out-of-plane magnetization. Comparing the top and bottom, we obtain the proof for $\rho_{yx}^o = 0$. In contrast to the above rather artificial setup, practically, we might have to foresee that the anomalous Hall effect would be flipped through the sweep $B_{xy} \rightarrow -B_{xy}$ due to potential field-misalignment towards the out-of-plane direction. This causes the apparent field-odd response of ρ_{yx} , but it should not be interpreted as the intrinsic in-plane Hall effect.

6' $\rho_{yx}^o(B_x, B_y, 0)$ is zero if there is a m in the xy plane in zero field unless the applied field flips the spontaneous magnetization.

We can apply the above discussion as shown in Fig. S2(b). The mirror inversion with m_{xy} transforms from the top to the middle with the reversal of the internal magnetic moments to $\mathcal{R}S_{A/B}$ and the B_{xy} . The B_{xy} -field inversion gives the bottom panel, where $S_{A/B}$ goes back to the original configuration. Only the E_y^o is remained reversed to give the proof for $\rho_{yx}^o = 0$.

Lastly, we consider the remaining two cases: systems with symmetries $\mathcal{T}C_{2x}$ or $\mathcal{T}m_{yz}$ in zero field. These two symmetries also potentially allow the spontaneous out-of-plane magnetization and thus the anomalous Hall effect, ρ_{yx}^A , while the application of the B_x field breaks the symmetries. We can prove the following two rules in the same manner described above.

7' $\rho_{yx}^o(B_x, 0, 0)$ is zero if there is a $\mathcal{T}C_2$ along the x axis in zero field unless the applied field flips the spontaneous magnetization.

As shown by the top panel in Fig. S3(a), we consider whether E_y^o is zero in the magnetic material

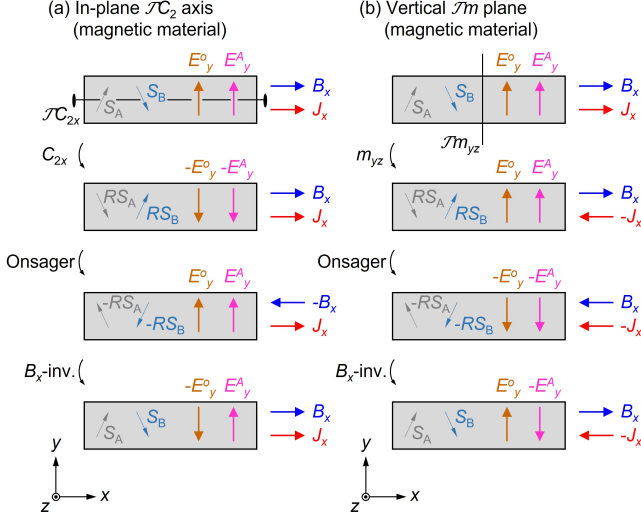


FIG. S3. Symmetry conditions 7' and 8' for the absence of the in-plane Hall effect in magnetic materials. See the caption of Figs. 2, S1, and S2 for details. (a) The case for the crystal with the \mathcal{TC}_{2x} rotational symmetry in zero field. Application of the C_{2x} rotation to the whole setup transforms the top to the second panel, which is accompanied by the inversion of E_y^o , and E_y^A . The magnetic moments are rotated to $\mathcal{RS}_{A/B}$. The Onsager's relation (Eq. (S4)) allows the transformation from the second to the third panel. The B_x -field inversion induces the transformation from the third panel to the bottom. (b) Corresponding figure for the crystal with the m_{xy} as the zero-field symmetry.

under J_x . Due to the applied B_x , the internal magnetic moments are canted to break \mathcal{TC}_{2x} symmetry for the zero field. Here, since the B along the exact x axis does not lift the degeneracy for the out-of-plane magnetization, we assume the possible anomalous Hall electric field E_y^A is maintained to be the same sign. We apply the C_{2x} rotation to the whole system to obtain the second panel, where the internal moments are also rotated to $\mathcal{RS}_{A/B}$ symbolically. The application of the Onsager's relation (Eq. (S4)) to the second panel leads to the third panel. Eventually, the B_x -field inversion leads to the bottom panel, where only the E_y^o is reversed by definition. We can safely assume that the internal moments rotate back to $S_{A/B}$ keeping the sign of E_y^A as the exact B_x field does not flip the out-of-plane magnetization. This can be known from the fact that, through the transformation from the top panel to the third, the possible out-of-plane magnetization is reversed twice by the C_{2x} and the Onsager's relation to recover into the original configuration. Comparing the top and the bottom, we obtain the proof for $\rho_{yx}^o = 0$.

8' $\rho_{yx}^o(B_x, 0, 0)$ is zero if there is a \mathcal{Tm} in the yz plane in zero field unless the applied field flips the spon-

taneous magnetization.

We can apply the same steps as described above to Fig. S3(b). The top panel is equivalent to the bottom panel, where E_y^o is unchanged even though the J_x is reversed. This means the $\rho_{yx}^o = 0$.

On the basis of the forbidden rules derived above, we can deduce the magnetic point groups that allow the in-plane Hall effect as summarized in Table I [91]. For example, the (magnetic) monoclinic $2/m$ does not show the finite $\rho_{xz}^o(B_x, B_y, 0)$ aside from the anomalous Hall effect ρ_{xz}^A due to $M \parallel y$ because of the presence of the m_{xz} (and C_{2y} as well), while it allows $\rho_{yx}^o(B_x)$. As for the tetragonal point group $4'$ with the \mathcal{TC}_4 rotation along the z axis, we can prove $\rho_{yx}^o(B_x, B_y, 0) = 0$ because the operation of the \mathcal{TC}_4 rotation twice is equivalent with C_2 along the z axis. We note that \mathcal{TC}_4 does not allow ρ_{yx}^A either in contrast to the $2/m$ case. The in-plane Hall effect is allowed for $\rho_{xz}^o(B_x)$, but forbidden for $\rho_{xz}^o(B_z)$ because B_z is parallel to the \mathcal{TC}_4 axis.

Similarly to the crystal twin discussed in the main text, different types of twin is expected in magnetic system, i.e., magnetic domains with respect to the time reversal. In contrast to the former, the reversal of the magnetic moments does not affect the sign of the in-plane Hall effect. We put the in-plane Hall resistivity as $\rho_{yx}^o(S_A + \delta s_A, S_B + \delta s_B, B_x)$, where $S_{A/B}$ are the symbolic sublattice moments and $\delta s_{A/B}$ are the B_x -induced canting towards the field (see Ref. [43] for detail). We apply the Onsager's relation Eq. (S4) to obtain

$$\begin{aligned}
 & \rho_{yx}^o(S_A + \delta s_A, S_B + \delta s_B, B_x) \\
 &= \rho_{xy}^o(-S_A - \delta s_A, -S_B - \delta s_B, -B_x) \\
 &= -\rho_{yx}^o(-S_A - \delta s_A, -S_B - \delta s_B, -B_x) \\
 &= \rho_{yx}^o(-S_A + \delta s_A, -S_B + \delta s_B, B_x). \quad (\text{S5})
 \end{aligned}$$

In the last equation, we assume that the B_x -field inversion only cause the sign change of $\delta s_{A/B}$. Comparing the first and the last equation, we obtain that the sign of the sublattice magnetic moments does not affect the in-plane Hall effect.

The magnetic half-Heusler compound DyPtBi is an example showing the in-plane Hall effect [35]. The crystal structure belongs to $\bar{4}3m$ in a paramagnetic state and the antiferromagnetic order breaks the time reversal symmetry. The in-plane Hall effect is allowed in the (111) plane with the current along the $[1\bar{1}0]$ axis and the magnetic field is away from the current direction as long as the mirror symmetry in the (110) plane is maintained. The observed signal for the field parallel to the current ($J \parallel B \parallel [1\bar{1}0]$) suggests a symmetry breaking of $m \perp [1\bar{1}0]$ due to a possible field-induced canted spin texture. Further analysis of the magnetic structure would be useful to identify the symmetry breaking that enhances the in-plane Hall effect in this system.

B. EFFECT OF OUT-OF-PLANE TRANSPORT TO THE VALIDITY OF $\hat{\sigma}_{2D}$ AND $\hat{\rho}_{2D}$

In this section, we discuss how to justify the approximation of the 2×2 matrices for the 3×3 matrices of $\hat{\rho}$

$$\hat{\rho}_{2/m}(B_x) = \frac{1}{\Delta_\sigma} \begin{pmatrix} \sigma_{yy}^e \sigma_{zz}^e + (\sigma_{yz}^o)^2 & -\sigma_{xy}^o \sigma_{zz}^e - \sigma_{yz}^o \sigma_{xz}^e & \sigma_{xy}^o \sigma_{yz}^o - \sigma_{yy}^e \sigma_{xz}^e \\ \sigma_{xy}^o \sigma_{zz}^e + \sigma_{yz}^o \sigma_{xz}^e & \sigma_{xx}^e \sigma_{zz}^e - (\sigma_{xz}^e)^2 & -\sigma_{yz}^o \sigma_{xx}^e - \sigma_{xy}^o \sigma_{xz}^e \\ \sigma_{xy}^o \sigma_{yz}^o - \sigma_{yy}^e \sigma_{xz}^e & \sigma_{yz}^o \sigma_{xx}^e + \sigma_{xy}^o \sigma_{xz}^e & \sigma_{xx}^e \sigma_{yy}^e + (\sigma_{xy}^o)^2 \end{pmatrix} \quad (\text{S6})$$

where Δ_σ is expressed as

$$\Delta_\sigma = \sigma_{xx}^e \sigma_{yy}^e \sigma_{zz}^e + \sigma_{xy}^o \sigma_{yz}^o \sigma_{xz}^e + \sigma_{xy}^o \sigma_{yz}^o \sigma_{xz}^e - \sigma_{yy}^e (\sigma_{xz}^e)^2 + (\sigma_{yz}^o)^2 \sigma_{xx}^e + (\sigma_{xy}^o)^2 \sigma_{zz}^e \quad (\text{S7})$$

Here, we assume that the field-odd Hall components, σ_{xy}^o and σ_{yz}^o are small compared to the field-even quantities, and set the quadratic form to be zero, e.g., $(\sigma_{xy}^o)^2 = 0$. The Δ_σ is approximated as follows:

$$\Delta_\sigma \sim \sigma_{xx}^e \sigma_{yy}^e \sigma_{zz}^e - \sigma_{yy}^e (\sigma_{xz}^e)^2 = \sigma_{xx}^e \sigma_{yy}^e \sigma_{zz}^e (1 - \tan \phi_{ex} \tan \phi_{ez}) \quad (\text{S8})$$

We introduce two pseudo Hall angles, $\phi_{ex} = \arctan(\sigma_{xz}^e / \sigma_{xx}^e)$ and $\phi_{ez} = \arctan(\sigma_{xz}^e / \sigma_{zz}^e)$. The form of Δ_σ can be understood as being corrected from the off-diagonal-free form $\sigma_{xx}^e \sigma_{yy}^e \sigma_{zz}^e$ by $1 - \tan \phi_{ex} \tan \phi_{ez}$. The correction is negligible when $\tan \phi_{ex} \ll 1$ in a quasi-two-dimensional system, and Eq. (6) is reduced to $\rho_{yx}^o = \sigma_{xy}^o / (\sigma_{xx}^e \sigma_{yy}^e)$, ensuring a direct proportionality between the in-plane Hall resistivity and conductivity.

Here, we discuss the form of $\hat{\sigma}$ as the inverse matrix of $\hat{\rho}$. The Δ_ρ is defined as the determinant of $\hat{\rho}$, and is approximated by

$$\Delta_\rho \sim \rho_{xx}^e \rho_{yy}^e \rho_{zz}^e - \rho_{yy}^e (\rho_{zx}^e)^2 = \rho_{xx}^e \rho_{yy}^e \rho_{zz}^e (1 - \tan \theta_{ex} \tan \theta_{ez}) \quad (\text{S9})$$

We introduce $\theta_{ex} = \arctan(\rho_{zx}^e / \rho_{xx}^e)$ and $\theta_{ez} = \arctan(\rho_{zx}^e / \rho_{zz}^e)$. Similar to Δ_σ , the Δ_ρ is corrected from $\rho_{xx}^e \rho_{yy}^e \rho_{zz}^e$ by $1 - \tan \theta_{ex} \tan \theta_{ez}$. The conductivity tensor components, σ_{xx}^e , σ_{yy}^e , and σ_{xy}^o are obtained

$$\sigma_{xx}^e \sim 1 / [\rho_{xx}^e (1 - \tan \theta_{ex} \tan \theta_{ez})], \quad (\text{S10})$$

$$\sigma_{yy}^e \sim 1 / \rho_{yy}^e, \quad (\text{S11})$$

and

$$\sigma_{xy}^o \sim (\rho_{yx}^o + \rho_{zx}^e \rho_{zy}^o / \rho_{zz}^e) / [\rho_{xx}^e \rho_{yy}^e (1 - \tan \theta_{ex} \tan \theta_{ez})]. \quad (\text{S12})$$

Compared to the quasi-two-dimensional forms (Eqs. (10) and (11)), both σ_{xx}^e and σ_{xy}^o gets a correction in the denominator due to the crystalline planar Hall effect (ρ_{zx}^e),

and $\hat{\sigma}$. We provide the explicit form of the $\hat{\rho}$ in Eq. (5), as the inverse matrix of $\hat{\sigma}$ in Eq. (4):

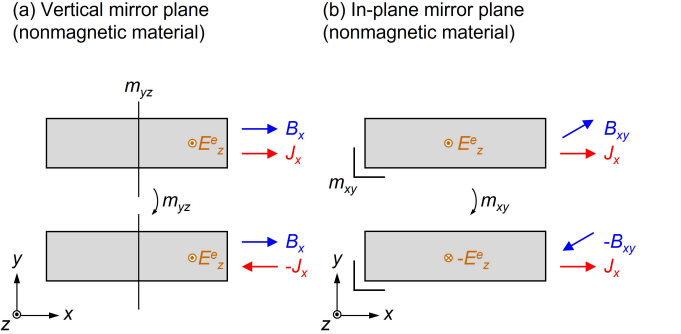


FIG. S4. Symmetry conditions for the absence of the crystalline planar Hall effect. See the caption of Fig. 2 for details. The orange circle with a dot or a cross represents a tentative crystalline planar Hall electric field $\pm E_z^e$ proportional to ρ_{zx}^e , which is proved to be zero. (a) The mirror inversion m_{yz} transforms the top to the bottom, which is accompanied with the inversion of J_x , but B_x and E_z^e remain intact. (b) Corresponding figure for the crystal with the m_{xy} symmetry.

which could be negligible in quasi-two-dimensional systems for $\tan \theta_{ez} \ll 1$, i.e., ρ_{zz}^e is large. As for the σ_{xy}^o , the numerator in Eq. (S12) also gets a correction by the leakage from the Hall effect ρ_{zy}^o in the yz plane. The two-dimensional approximation of the σ_{xy}^o (Eq. (11)) is valid only if $\rho_{zx}^e \rho_{zy}^o / \rho_{zz}^e$ is negligible. This is realized in quasi-two-dimensional systems with low out-of-plane carrier (electrons/phonons/magnons, etc.) mobility giving a small out-of-plane normal-Hall-angle $\rho_{zy}^o / \rho_{zz}^e$.

C. SYMMETRY CONDITIONS FOR NON-ZERO ρ_{zx}^e

As suggested in the main text, the out-of-plane transport inevitably contaminates the in-plane Hall signal through the potentially finite σ_{xz}^e . Henceforth, we refer to σ_{xz}^e (ρ_{zx}^e) as the crystalline planar Hall conductivity (resistivity). Indeed, we can prove that the conditions for the non-zero $\rho_{zx}^e(B_x, B_y, 0)$ (and $\sigma_{xz}^e(B_x, B_y, 0)$) are equivalent to those for the $\rho_{yx}^o(B_x, B_y, 0)$ by using the pictorial approaches regarding Figs. 2 and S1-S3.

To avoid repeating similar explanations, we show only representative cases. One example is a vertical mirror symmetry in the yz plane (see Fig. S4(a)). Here, we consider that a tentative out-of-plane electric field E_z^e is induced by the application of J_x , which is proved to be zero. The mirror operation transforms the system from the top to the bottom, where the B_x and E_z^e remain intact, but the J_x is reversed. This relationship is expressed as $E_z^e = \rho_{xz}^e(B_x, 0, 0) \cdot J_x = \rho_{xz}^e(B_x, 0, 0) \cdot (-J_x)$, and thus $\rho_{xz}^e(B_x, 0, 0) = 0$. The other example is a horizontal mirror symmetry in the xy plane (see Fig. S4(b)). The mirror inversion reverses E_z^e , and B_{xy} to give the equation $E_z^e = \rho_{xz}^e(B_x, B_y, 0) \cdot J_x = -\rho_{xz}^e(-B_x, -B_y, 0) \cdot J_x$. We note that $\rho_{xz}^e(B_x, B_y, 0) = \rho_{xz}^e(-B_x, -B_y, 0)$, and thus obtain the proof of $\rho_{xz}^e(B_x, B_y, 0)$. We can straightforwardly prove the other conditions for the absence of $\rho_{xz}^e(B_x, B_y, 0)$.

The leading order in terms of B for ρ_{xz}^e (and σ_{xz}^e as well) depends on the crystal symmetry. Triclinic and monoclinic systems are $\rho_{xz}^e \neq 0$ even in zero field. Other point groups start from $\rho_{xz}^e \propto B^2$ since it originates from the anisotropy of magnetoresistance, which is zero at $B = 0$.

D. THERMAL TRANSPORT MEASUREMENTS AND TWIN OPERATIONS OF α -RUCL₃

In Table II, we show a list of published literature reporting the thermal transport properties of α -RuCl₃. Each row summarizes the experimental conditions (heat current and magnetic field direction), the equations, either Eq. (13) or (14), used to estimate the thermal Hall conductivity, and growth methods for single crystals.

Figure S5(a) shows the proposed crystal structure of the $R\bar{3}$ RuCl₃ [76, 82, 83], which is described by the stacking of Cl-Ru-Cl layers along the $[111]_r$ (r denotes the rhombohedral lattice) in the order of A , B , and C (see Fig. S5(b)). Each layer can be completely superimposed by a pure spatial translation of $[100]_r$. As the $R\bar{3}$ lattice does not have the symmetries, C_{2z} , m_{xz} , and m_{yz} , three different types of twin domains associated with the stacking faults can be considered. Figure S5(c) shows the crystal structure after the C_{2z} operation. The ABC stacking is converted to the CBA stacking and the rhombohedral unit cell is changed to the reverse setting (see the orientation of the unit cell). As we discussed the symmetry condition for the in-plane Hall effect in Fig. 2(c), the C_{2z} rotation reverses the sign of the $\kappa_{xy}^o(B_x)$ (< 0). A similar discussion can also be applied to the m_{xz} and m_{yz} operations as summarized in Figs. S5(b) and S5(c), respectively. We note that, in contrast to the case of the triangular lattice considered in Fig. 3(c), the obverse-reverse twinning (twinning by reticular merohedry) is irrelevant for the sign reversal of the κ_{xy}^o . This occurs between the ferroaxial domains [84, 85] in the same obverse-

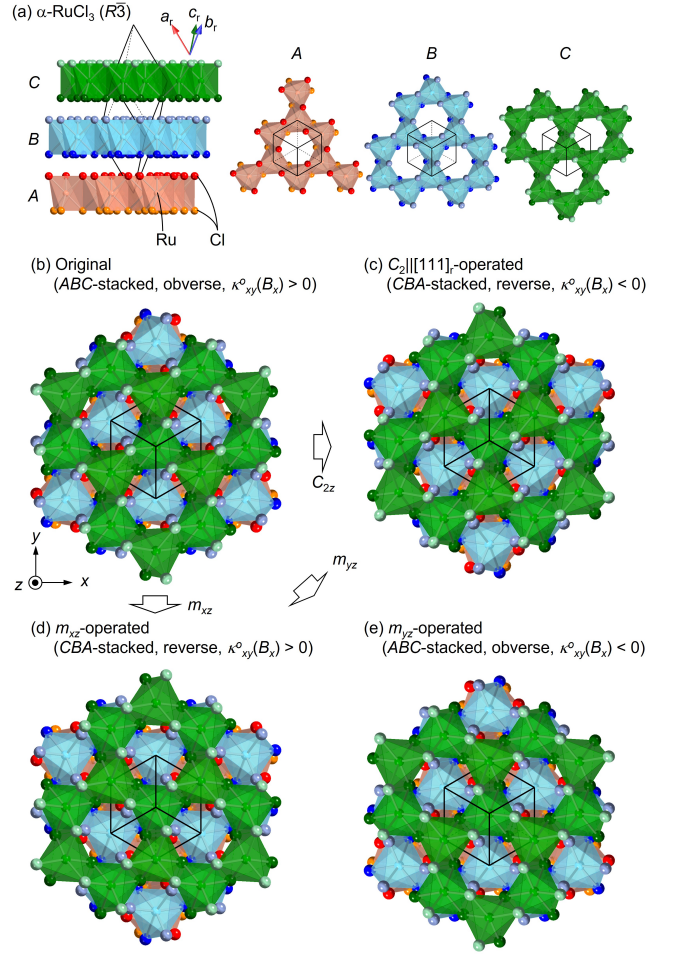


FIG. S5. (a) Left: The proposed crystal structure of α -RuCl₃ at low temperature [76], which belongs to the $R\bar{3}$ space group. Right: top view of the three types of Cl-Ru-Cl honeycomb layer of different orientations denoted as A , B , and C . Displacement of the atomic position of chlorine from the symmetric position is exaggerated for visibility. The black line is the unit cell in the rhombohedral axes. (b) Top view of the original $R\bar{3}$ crystal structure, characterized by the ABC stacking and the obverse setting. The Cartesian coordinate, xyz , is defined, and the expected thermal Hall conductivity $\kappa_{xy}^o(B_x)$ is set to be positive. (c)-(d) Possible twin domains produced by the twin operations: C_{2z} for (c), m_{xz} for (d), and m_{yz} for (e). The stacking order (ABC or CBA), the lattice setting (obverse and reverse), and the sign of the $\kappa_{xy}^o(B_x)$ are also shown.

reverse settings, which can be identified by electrogyration [92, 93], and electron/x-ray diffraction [94].

TABLE II. Experimental conditions of the thermal transport measurements for α -RuCl₃. $\perp z$ for the heat current direction indicates no specification of the crystallographic axis. Accordingly, the measured thermal conductivity is denoted by κ_{\perp} instead of κ_{xx} or κ_{yy} . There are two ways, exact and approximate, to experimentally estimate κ_{xy} according to Eqs. (13) and (14), respectively. Due to the lack of consensus on the low-temperature crystal structure, we provisionally hypothesize the in-plane isotropy for the $B \parallel z$ measurements (marked with an asterisk).

No.	Heat current	Magnetic field	Measured components	Form of κ_{xy}	Growth method	Ref.
1.	$\perp z$	NA	κ_{\perp}	NA	Bridgman	95
2.	$\perp z$	$\perp z, \parallel J$	κ_{\perp}	NA	vacuum sublimation	96
	$\perp z$	$\perp z, \perp J$	κ_{\perp}	NA		
3.	$\perp z$	$\parallel z$	$\kappa_{\perp}, \kappa_{xy}$	exact*	Bridgman	97
4.	$\perp z$	$\perp z, \perp J$	κ_{\perp}	NA	CVT	98
5.	$\perp z$	$\perp z, \perp J$	κ_{\perp}	NA	CVT/vacuum sublimation	88
	$\parallel z$	$\perp z, \perp J$	κ_{zz}	NA		
6.	$\parallel x$	toward x from z by 60° and 45°	κ_{xx}, κ_{xy}	approximate	Bridgman	37
7.	$\perp z$	$\parallel z$	$\kappa_{\perp}, \kappa_{xy}$	exact*	CVT	99
8.	$\perp z$	$\perp z, \perp J$	κ_{\perp}	NA	CVT	100
9.	$\parallel x$	toward x from z by 45°	κ_{xx}, κ_{xy}	approximate	Bridgman	65
10.	$\perp z$	$\parallel x$	$\kappa_{\perp}, \kappa_{xy}$	approximate	CVT	68
	$\perp z$	$\parallel y$	$\kappa_{\perp}, \kappa_{xy}$	approximate		
11.	$\parallel x$	$\parallel x$	κ_{xx}, κ_{xy}	approximate	Bridgman	38
	$\parallel x$	$\parallel y$	κ_{xx}, κ_{xy}	approximate		
12.	$\parallel x$	$\parallel z$	κ_{xx}, κ_{xy}	exact*	CVT	40
	$\parallel x$	toward x from z	κ_{xx}, κ_{xy}	approximate		
13.	$\parallel x$	$\parallel x$	κ_{xx}, κ_{xy}	approximate	CVT	39
14.	$\parallel x$	NA	κ_{\perp}	NA	Bridgman	64
15.	$\parallel x$	$\parallel x$	κ_{xx}, κ_{xy}	approximate	Bridgman	71
	$\parallel x$	$\parallel y$	κ_{xx}, κ_{xy}	approximate		
16.	$\parallel x$	$\parallel x$	κ_{xx}	NA	Bridgman	69
	$\parallel x$	$\parallel y$	κ_{xx}	NA	Bridgman	
	$\parallel x$	$\parallel x$	κ_{xx}	NA	CVT	
	$\parallel x$	$\parallel y$	κ_{xx}	NA	CVT	
17.	$\parallel x$	toward x from z	κ_{xx}, κ_{xy}	approximate	Bridgman	66
18.	$\parallel x$	$\parallel x$ and $\parallel y$	κ_{xx}	NA	CVT	70
	$\parallel y$	$\parallel x$ and $\parallel y$	κ_{yy}	NA		
19.	$\parallel x$	$\parallel x$	κ_{xx}, κ_{xy}	approximate	CVT	101
20.	$\parallel x$	$\parallel x$	κ_{xx}, κ_{xy}	approximate	CVT	102

-
- [1] C. Hurd, *The Hall effect in metals and alloys* (Springer, 1972).
- [2] C. Goldberg and R. E. Davis, “New galvanomagnetic effect,” *Phys. Rev.* **94**, 1121 (1954).
- [3] K. M. Koch, “Zum problem der galvanomagnetischen effekte in ferromagneticis,” *Z. Naturforsch A* **10**, 496 (1955).
- [4] V. D. Ky, “Plane Hall effect in ferromagnetic metals,” *Sov. Phys. JETP* **23**, 809 (1966).
- [5] J.-P. Jan, “Galvanomagnetic and thermomagnetic effects in metals,” in *Solid State Physics*, Vol. 5 (Elsevier, 1957) p. 1.
- [6] Equivalently, the in-plane Hall effect is defined as the Hall electric field parallel to the magnetic field ($B_x \parallel E_x$) when the current (J_y) is applied perpendicular to B_x (see Fig. 5(c)).
- [7] F. Garcia-Moliner, “A variational calculation of electronic transport in a magnetic field,” *Proc. Roy. Soc. Lond. A* **249**, 73 (1959).
- [8] L. Grabner, “Longitudinal Hall effect,” *Phys. Rev.* **117**, 689 (1960).
- [9] T. Okada, “The measurement of the galvanomagnetic tensors of bismuth,” *J. Phys. Soc. Jpn.* **11**, 89 (1956).
- [10] T. Okada, “The measurements of the galvanomagnetic tensors of bismuth,” *J. Phys. Soc. Jpn.* **12**, 1327 (1957).
- [11] M. Möllendorf and W. Bauhofer, “First-order longitudinal Hall effect,” *Phys. Rev. B* **30**, 1099 (1984).
- [12] W. Bauhofer, “Two-band character of the first-order longitudinal Hall effect,” *Phys. Rev. B* **38**, 5215 (1988).
- [13] M. S. Bresler and N. A. Red’ko, “Galvanomagnetic phenomena in antimony at low temperatures,” *Sov. Phys. JETP* **34**, 149 (1972).
- [14] Y. C. Akgoz and G. A. Saunders, “Galvanomagnetic effects of arsenic (25.5 at%)–antimony alloy single crystals,” *J. Phys. C: Solid State Phys.* **7**, 1655 (1974).
- [15] W. Bauhofer, “Longitudinal Hall effect in SrAs₃,” *Phys. Rev. B* **32**, 1183 (1985).
- [16] R. v. Baltz, W. Denk, and W. Bauhofer, “Theoretical investigation of the longitudinal Hall effect in SrAs₃,” *Phys. Rev. B* **48**, 2098 (1993).
- [17] P. J. Klar and W. Bauhofer, “Galvanomagnetic properties and band structure of monoclinic SrAs₃,” *Phys. Rev. B* **50**, 5180 (1994).
- [18] Y. Zhang and C. Zhang, “Quantized anomalous Hall insulator in a nanopatterned two-dimensional electron gas,” *Phys. Rev. B* **84**, 085123 (2011).
- [19] X. Liu, H.-C. Hsu, and C.-X. Liu, “In-plane magnetization-induced quantum anomalous Hall effect,” *Phys. Rev. Lett.* **111**, 086802 (2013).
- [20] Y. Ren, J. Zeng, X. Deng, F. Yang, H. Pan, and Z. Qiao, “Quantum anomalous Hall effect in atomic crystal layers from in-plane magnetization,” *Phys. Rev. B* **94**, 085411 (2016).
- [21] X.-L. Sheng and B. K. Nikolić, “Monolayer of the 5d transition metal trichloride OsCl₃: A playground for two-dimensional magnetism, room-temperature quantum anomalous Hall effect, and topological phase transitions,” *Phys. Rev. B* **95**, 201402 (2017).
- [22] P. Zhong, Y. Ren, Y. Han, L. Zhang, and Z. Qiao, “In-plane magnetization-induced quantum anomalous Hall effect in atomic crystals of group-V elements,” *Phys. Rev. B* **96**, 241103 (2017).
- [23] J. Zhang, Z. Liu, and J. Wang, “In-plane magnetic-field-induced quantum anomalous Hall plateau transition,” *Phys. Rev. B* **100**, 165117 (2019).
- [24] Z. Liu, G. Zhao, B. Liu, Z. F. Wang, J. Yang, and F. Liu, “Intrinsic quantum anomalous Hall effect with in-plane magnetization: searching rule and material prediction,” *Phys. Rev. Lett.* **121**, 246401 (2018).
- [25] Z. Li, Y. Han, and Z. Qiao, “Chern number tunable quantum anomalous Hall effect in monolayer transitional metal oxides via manipulating magnetization orientation,” *Phys. Rev. Lett.* **129**, 036801 (2022).
- [26] A. G. Mal’shukov, K. A. Chao, and M. Willander, “Hall effect in a magnetic field parallel to interfaces of a III-V semiconductor quantum well,” *Phys. Rev. B* **57**, R2069 (1998).
- [27] V. A. Zyuzin, “In-plane Hall effect in two-dimensional helical electron systems,” *Phys. Rev. B* **102**, 241105 (2020).
- [28] R. Battilomo, N. Scopigno, and C. Ortix, “Anomalous planar Hall effect in two-dimensional trigonal crystals,” *Phys. Rev. Research* **3**, L012006 (2021).
- [29] S. Sun, H. Weng, and X. Dai, “Possible quantization and half-quantization in the anomalous Hall effect caused by in-plane magnetic field,” *Phys. Rev. B* **106**, L241105 (2022).
- [30] J. H. Cullen, P. Bhalla, E. Marcellina, A. R. Hamilton, and D. Culcer, “Generating a topological anomalous Hall effect in a nonmagnetic conductor: An in-plane magnetic field as a direct probe of the Berry curvature,” *Phys. Rev. Lett.* **126**, 256601 (2021).
- [31] H. Tan, Y. Liu, and B. Yan, “Unconventional anomalous Hall effect from magnetization parallel to the electric field,” *Phys. Rev. B* **103**, 214438 (2021).
- [32] H. Wang, Y.-X. Huang, H. Liu, X. Feng, J. Zhu, W. Wu, C. Xiao, and S. A. Yang, “Theory of intrinsic in-plane Hall effect,” arXiv preprint arXiv:2211.05978 (2022).
- [33] T. Liang, J. Lin, Q. Gibson, S. Kushwaha, M. Liu, W. Wang, H. Xiong, J. A. Sobota, M. Hashimoto, P. S. Kirchmann, *et al.*, “Anomalous Hall effect in ZrTe₅,” *Nat. Phys.* **14**, 451 (2018).
- [34] J. Zhou, W. Zhang, Y.-C. Lin, J. Cao, Y. Zhou, W. Jiang, H. Du, B. Tang, J. Shi, B. Jiang, *et al.*, “Heterodimensional superlattice with in-plane anomalous Hall effect,” *Nature* **609**, 46 (2022).
- [35] J. Chen, H. Li, B. Ding, P. Chen, T. Guo, X. Xu, D. Zheng, H. Zhang, X. Xi, and W. Wang, “Unconventional anomalous Hall effect in the canted antiferromagnetic half-Heusler compound DyPtBi,” *Adv. Funct. Mater.* **32**, 2107526 (2022).
- [36] A. Kitaev, “Anyons in an exactly solved model and beyond,” *Ann. Phys.* **321**, 2 (2006).
- [37] Y. Kasahara, T. Ohnishi, Y. Mizukami, O. Tanaka, S. Ma, K. Sugii, N. Kurita, H. Tanaka, J. Nasu, Y. Motome, *et al.*, “Majorana quantization and half-integer thermal quantum Hall effect in a Kitaev spin liquid,” *Nature* **559**, 227 (2018).
- [38] T. Yokoi, S. Ma, Y. Kasahara, S. Kasahara, T. Shibauchi, N. Kurita, H. Tanaka, J. Nasu, Y. Motome, C. Hickey, *et al.*, “Half-integer quantized anomalous thermal Hall effect in the Kitaev material candidate α -RuCl₃,” *Science* **373**, 568 (2021).
- [39] P. Czajka, T. Gao, M. Hirschberger, P. Lampen-Kelley, A. Banerjee, N. Quirk, D. Mandrus, S. Nagler, and

- N. P. Ong, “Planar thermal Hall effect of topological bosons in the Kitaev magnet α -RuCl₃,” *Nat. Mater.* **22**, 36 (2022).
- [40] É. Lefrançois, G. Grissonnanche, J. Baglo, P. Lampen-Kelley, J.-Q. Yan, C. Balz, D. Mandrus, S. E. Nagler, S. Kim, Y.-J. Kim, *et al.*, “Evidence of a phonon Hall effect in the Kitaev spin liquid candidate α -RuCl₃,” *Phys. Rev. X* **12**, 021025 (2022).
- [41] H. J. Juretschke, “Symmetry of galvanomagnetic effects in antimony,” *Acta Cryst.* **8**, 716 (1955).
- [42] Y. C. Akgoz and G. A. Saunders, “Space-time symmetry restrictions on the form of transport tensors. I. Galvanomagnetic effects,” *J. Phys. C: Solid State Physics* **8**, 1387 (1975).
- [43] H. Grimmer, “General relations for transport properties in magnetically ordered crystals,” *Acta Cryst. A* **49**, 763 (1993).
- [44] I. M. B. de Figueiredo and R. E. Raab, “A pictorial approach to macroscopic space-time symmetry, with particular reference to light scattering,” *Proc. R. Soc. Lond. A* **369**, 501 (1980).
- [45] H. Takeda, J. Mai, M. Akazawa, K. Tamura, J. Yan, K. Moovendaran, K. Raju, R. Sankar, K.-Y. Choi, and M. Yamashita, “Planar thermal Hall effects in the Kitaev spin liquid candidate Na₂Co₂TeO₆,” *Phys. Rev. Research* **4**, L042035 (2022).
- [46] The *Hall* effect is often used to describe only field-odd transverse responses [5, 27, 103], but phenomenologically it is more generally defined as being independent of the field-reversal symmetry [47, 104].
- [47] L. P. Kao and E. Katz, “Phenomenological theory of anisotropic isothermal galvanomagnetic effects,” *J. Phys. Chem. Solids* **6**, 223 (1958).
- [48] A. C. Smith, J. F. Janak, and R. B. Adler, *Electronic conduction in solids* (McGraw-Hill, New York, 1967).
- [49] F. G. Utermohlen and N. Trivedi, “Symmetry analysis of tensors in the honeycomb lattice of edge-sharing octahedra,” *Physical Review B* **103**, 155124 (2021).
- [50] D. Szaller, S. Bordács, and I. Kézsmárki, “Symmetry conditions for nonreciprocal light propagation in magnetic crystals,” *Phys. Rev. B* **87**, 014421 (2013).
- [51] S.-W. Cheong, “SOS: symmetry-operational similarity,” *npj Quantum Mater.* **4**, 1 (2019).
- [52] T. Kurumaji, “Spiral spin structures and skyrmions in multiferroics,” *Phys. Sci. Rev.* **5** (2020).
- [53] S. Parsons, “Introduction to twinning,” *Acta Cryst. D* **59**, 1995 (2003).
- [54] In a single-carrier system, it can be proved that those two terms in Eq. (6) completely cancel with each other [15] unless the Berry curvature has finite contribution. In two-carrier system, this cancellation is imperfect due to mobility difference.
- [55] I. Isenberg, B. R. Russell, and R. F. Greene, “Improved method for measuring Hall coefficients,” *Rev. Sci. Instr.* **19**, 685 (1948).
- [56] J. R. Drabble and R. Wolfe, “Geometrical effects in transverse magnetoresistance measurements,” *Intl. J. Electronics* **3**, 259 (1957).
- [57] S. Mumford, T. Paul, E. Kountz, and A. Kapitulnik, “Sample shape and boundary dependence of measured transverse thermal properties,” *J. Appl. Phys.* **128**, 175105 (2020).
- [58] A. Gourgout, M. Leroux, J.-L. Smirr, M. Massouzdégan, R. P. S. M. Lobo, D. Vignolles, C. Proust, H. Berger, Q. Li, G. Gu, *et al.*, “Magnetic freeze-out and anomalous Hall effect in ZrTe₅,” *npj Quantum Mater.* **7**, 1 (2022).
- [59] J. Fujioka, R. Yamada, M. Kawamura, S. Sakai, M. Hirayama, R. Arita, T. Okawa, D. Hashizume, M. Hoshino, and Y. Tokura, “Strong-correlation induced high-mobility electrons in Dirac semimetal of perovskite oxide,” *Nat. Commun.* **10**, 1 (2019).
- [60] J. Ge, D. Ma, Y. Liu, H. Wang, Y. Li, J. Luo, T. Luo, Y. Xing, J. Yan, D. Mandrus, *et al.*, “Unconventional Hall effect induced by Berry curvature,” *Natl. Sci. Rev.* **7**, 1879 (2020).
- [61] A. K. Nayak, J. E. Fischer, Y. Sun, B. Yan, J. Karel, A. C. Komarek, C. Shekhar, N. Kumar, W. Schnelle, J. Kübler, *et al.*, “Large anomalous Hall effect driven by a nonvanishing Berry curvature in the noncolinear antiferromagnet Mn₃Ge,” *Sci. Adv.* **2**, e1501870 (2016).
- [62] M. Hirschberger, S. Hayami, and Y. Tokura, “Nanomeric skyrmion lattice from anisotropic exchange interactions in a centrosymmetric host,” *New J. Phys.* **23**, 023039 (2021).
- [63] M. S. Alam, A. Fakhredine, M. Ahmed, P. K. Tanwar, H.-Y. Yang, F. Tafti, G. Cuono, R. Islam, B. Singh, A. Lynnyk, *et al.*, “Sign change of anomalous Hall effect and anomalous Nernst effect in the Weyl semimetal CeAlSi,” *Phys. Rev. B* **107**, 085102 (2022).
- [64] J. A. N. Bruin, R. R. Claus, Y. Matsumoto, N. Kurita, H. Tanaka, and H. Takagi, “Robustness of the thermal Hall effect close to half-quantization in α -RuCl₃,” *Nat. Phys.* **18**, 401 (2022).
- [65] M. Yamashita, J. Gouchi, Y. Uwatoko, N. Kurita, and H. Tanaka, “Sample dependence of half-integer quantized thermal Hall effect in the Kitaev spin-liquid candidate α -RuCl₃,” *Phys. Rev. B* **102**, 220404 (2020).
- [66] Y. Kasahara, S. Suetsugu, T. Asaba, S. Kasahara, T. Shibauchi, N. Kurita, H. Tanaka, and Y. Matsuda, “Quantized and unquantized thermal Hall conductance of Kitaev spin-liquid candidate α -RuCl₃,” *Phys. Rev. B* **106** (2022).
- [67] J. Nasu, J. Yoshitake, and Y. Motome, “Thermal transport in the Kitaev model,” *Phys. Rev. Lett.* **119**, 127204 (2017).
- [68] P. Czajka, T. Gao, M. Hirschberger, P. Lampen-Kelley, A. Banerjee, J. Yan, D. G. Mandrus, S. E. Nagler, and N. P. Ong, “Oscillations of the thermal conductivity in the spin-liquid state of α -RuCl₃,” *Nat. Phys.* **17**, 915 (2021).
- [69] J. A. N. Bruin, R. R. Claus, Y. Matsumoto, J. Nuss, S. Laha, B. V. Lotsch, N. Kurita, H. Tanaka, and H. Takagi, “Origin of oscillatory structures in the magnetothermal conductivity of the putative Kitaev magnet α -RuCl₃,” *APL Mater* **10** (2022).
- [70] É. Lefrançois, J. Baglo, Q. Barthélemy, S. Kim, Y.-J. Kim, and L. Taillefer, “Oscillations in the magnetothermal conductivity of α -RuCl₃: Evidence of transition anomalies,” *Phys. Rev. B* **107**, 064408 (2023).
- [71] S. Suetsugu, Y. Ukai, M. Shimomura, M. Kamimura, T. Asaba, Y. Kasahara, N. Kurita, H. Tanaka, T. Shibauchi, J. Nasu, *et al.*, “Evidence for a phase transition in the quantum spin liquid state of a Kitaev candidate α -RuCl₃,” *J. Phys. Soc. Jpn.* **91**, 124703 (2022).
- [72] L. E. Chern, E. Z. Zhang, and Y. B. Kim, “Sign

- structure of thermal Hall conductivity and topological magnons for in-plane field polarized Kitaev magnets,” *Phys. Rev. Lett.* **126**, 147201 (2021).
- [73] E. Z. Zhang, L. E. Chern, and Y. B. Kim, “Topological magnons for thermal Hall transport in frustrated magnets with bond-dependent interactions,” *Phys. Rev. B* **103**, 174402 (2021).
- [74] S. Koyama and J. Nasu, “Field-angle dependence of thermal Hall conductivity in a magnetically ordered Kitaev-Heisenberg system,” *Phys. Rev. B* **104**, 075121 (2021).
- [75] O. Tanaka, Y. Mizukami, R. Harasawa, K. Hashimoto, K. Hwang, N. Kurita, H. Tanaka, S. Fujimoto, Y. Matsuda, E.-G. Moon, *et al.*, “Thermodynamic evidence for a field-angle-dependent Majorana gap in a Kitaev spin liquid,” *Nat. Phys.* **18**, 429 (2022).
- [76] S.-Y. Park, S.-H. Do, K.-Y. Choi, D. Jang, T.-H. Jang, J. Schefer, C.-M. Wu, J. S. Gardner, J. M. S. Park, J.-H. Park, *et al.*, “Emergence of the isotropic Kitaev honeycomb lattice with two-dimensional Ising universality in α - RuCl_3 ,” arXiv preprint arXiv:1609.05690 (2016).
- [77] S. Kim, B. Yuan, and Y.-J. Kim, “ α - RuCl_3 and other Kitaev materials,” *APL Mater.* **10**, 080903 (2022).
- [78] B. W. Lebert, S. Kim, D. A. Prishchenko, A. A. Tsirlin, A. H. Said, A. Alatas, and Y.-J. Kim, “Acoustic phonon dispersion of α - RuCl_3 ,” *Phys. Rev. B* **106** (2022).
- [79] H. B. Cao, A. Banerjee, J.-Q. Yan, C. A. Bridges, M. D. Lumsden, D. G. Mandrus, D. A. Tennant, B. C. Chakoumakos, and S. E. Nagler, “Low-temperature crystal and magnetic structure of α - RuCl_3 ,” *Phys. Rev. B* **93**, 134423 (2016).
- [80] M. C. Shapiro, A. T. Hristov, J. C. Palmstrom, J.-H. Chu, and I. R. Fisher, “Measurement of the B_{1g} and B_{2g} components of the elastoresistivity tensor for tetragonal materials via transverse resistivity configurations,” *Rev. Sci. Instr.* **87**, 063902 (2016).
- [81] P. Walmsley and I. R. Fisher, “Determination of the resistivity anisotropy of orthorhombic materials via transverse resistivity measurements,” *Rev. Sci. Instr.* **88**, 043901 (2017).
- [82] A. Glamazda, P. Lemmens, S.-H. Do, Y. S. Kwon, and K.-Y. Choi, “Relation between Kitaev magnetism and structure in α - RuCl_3 ,” *Phys. Rev. B* **95**, 174429 (2017).
- [83] S. Mu, K. D. Dixit, X. Wang, D. L. Abernathy, H. Cao, S. E. Nagler, J. Yan, P. Lampen-Kelley, D. Mandrus, C. A. Polanco, *et al.*, “Role of the third dimension in searching for Majorana fermions in α - RuCl_3 via phonons,” *Phys. Rev. Research* **4**, 013067 (2022).
- [84] V. Gopalan and D. B. Litvin, “Rotation-reversal symmetries in crystals and handed structures,” *Nat. Mater.* **10**, 376 (2011).
- [85] J. Hlinka, J. Privratska, P. Ondrejovic, and V. Janovec, “Symmetry guide to ferroaxial transitions,” *Phys. Rev. Lett.* **116**, 177602 (2016).
- [86] Y. Kubota, H. Tanaka, T. Ono, Y. Narumi, and K. Kindo, “Successive magnetic phase transitions in α - RuCl_3 : XY-like frustrated magnet on the honeycomb lattice,” *Phys. Rev. B* **91**, 094422 (2015).
- [87] R. D. Johnson, S. C. Williams, A. A. Haghighirad, J. Singleton, V. Zapf, P. Manuel, I. I. Mazin, Y. Li, H. O. Jeschke, R. Valentí, *et al.*, “Monoclinic crystal structure of α - RuCl_3 and the zigzag antiferromagnetic ground state,” *Phys. Rev. B* **92**, 235119 (2015).
- [88] R. Hentrich, A. U. B. Wolter, X. Zotos, W. Brenig, D. Nowak, A. Isaeva, T. Doert, A. Banerjee, P. Lampen-Kelley, D. G. Mandrus, *et al.*, “Unusual phonon heat transport in α - RuCl_3 : strong spin-phonon scattering and field-induced spin gap,” *Phys. Rev. Lett.* **120**, 117204 (2018).
- [89] T. Ideue, T. Kurumaji, S. Ishiwata, and Y. Tokura, “Giant thermal Hall effect in multiferroics,” *Nat. Mater.* **16**, 797 (2017).
- [90] S. Shtrikman and H. Thomas, “Remarks on linear magneto-resistance and magneto-heat-conductivity,” *Solid State Commun.* **3**, 147 (1965).
- [91] In Ref. [31], a similar table is also given, where ferromagnetic cases for each point group are considered, while the cubic groups are excluded without sufficient justification.
- [92] K. Aizu, “Reversal in optical rotatory power— ”gyroelectric” crystals and ”hypergyroelectric” crystals,” *Phys. Rev.* **133**, A1584 (1964).
- [93] A. S. Gupta, O. Arteaga, R. Haislmaier, B. Kahr, and V. Gopalan, “Reinvestigation of electric field-induced optical activity in α -quartz: Application of a polarimeter with four photoelastic modulators,” *Chirality* **26**, 430 (2014).
- [94] G. L. Nord Jr and C. A. Lawson, “Order-disorder transition-induced twin domains and magnetic properties in ilmenite-hematite,” *Am. Mineral.* **74**, 160 (1989).
- [95] D. Hirobe, M. Sato, Y. Shiomi, H. Tanaka, and E. Saitoh, “Magnetic thermal conductivity far above the Néel temperature in the Kitaev-magnet candidate α - RuCl_3 ,” *Phys. Rev. B* **95**, 241112 (2017).
- [96] I. A. Leahy, C. A. Pocs, P. E. Siegfried, D. Graf, S.-H. Do, K.-Y. Choi, B. Normand, and M. Lee, “Anomalous thermal conductivity and magnetic torque response in the honeycomb magnet α - RuCl_3 ,” *Phys. Rev. Lett.* **118**, 187203 (2017).
- [97] Y. Kasahara, K. Sugii, T. Ohnishi, M. Shimozawa, M. Yamashita, N. Kurita, H. Tanaka, J. Nasu, Y. Motome, T. Shibauchi, *et al.*, “Unusual thermal Hall effect in a Kitaev spin liquid candidate α - RuCl_3 ,” *Phys. Rev. Lett.* **120**, 217205 (2018).
- [98] Y. J. Yu, Y. Xu, K. J. Ran, J. M. Ni, Y. Y. Huang, J. H. Wang, J. S. Wen, and S. Y. Li, “Ultralow-temperature thermal conductivity of the Kitaev honeycomb magnet α - RuCl_3 across the field-induced phase transition,” *Phys. Rev. Lett.* **120**, 067202 (2018).
- [99] R. Hentrich, M. Roslova, A. Isaeva, T. Doert, W. Brenig, B. Büchner, and C. Hess, “Large thermal Hall effect in α - RuCl_3 : Evidence for heat transport by Kitaev-Heisenberg paramagnons,” *Phys. Rev. B* **99**, 085136 (2019).
- [100] R. Hentrich, X. Hong, M. Gillig, F. Caglieris, M. Čulo, M. Shahrokhvand, U. Zeitler, M. Roslova, A. Isaeva, T. Doert, *et al.*, “High-field thermal transport properties of the Kitaev quantum magnet α - RuCl_3 : Evidence for low-energy excitations beyond the critical field,” *Phys. Rev. B* **102**, 235155 (2020).
- [101] H. Zhang, A. May, H. Miao, B. Sales, D. Mandrus, S. Nagler, M. McGuire, and J. Yan, “The sample-dependent and sample-independent thermal transport properties of α - RuCl_3 ,” arXiv preprint arXiv:2303.02098 (2023).
- [102] H. Zhang, M. A. McGuire, A. F. May, J. Chao, Q. Zheng, M. Chi, B. C. Sales, D. G. Mandrus, S. E. Nagler, H. Miao, *et al.*, “Stacking disorder and ther-

- mal transport properties of α -RuCl₃,” arXiv preprint arXiv:2303.03682 (2023).
- [103] H. B. G. Casimir, “On Onsager’s principle of microscopic reversibility,” *Rev. Mod. Phys.* **17**, 343 (1945).
- [104] A. C. Beer, *Galvanomagnetic effects in semiconductors*, Vol. 4 (Academic Press, 1963).